Heliyon 10 (2024) e32992

Contents lists available at ScienceDirect

Heliyon

journal homepage: www.cell.com/heliyon

Research article

Comprehensive approach integrating remote sensing, machine learning, and physicochemical parameters to detect hydrodynamic conditions and groundwater quality deterioration in non-rechargeable aquifer systems

Mohamed Hamdy Eid [a,b,*], Ali Shebl [c,d], Mustafa Eissa [e,f], Essam A. Mohamed [g], Amr S. Fahil [h,i], Hatem Saad Ramadan [g], Mostafa R. Abukhadra [b], Ahmed M. El-Sherbeeny [j], Attila Kovacs [a], Péter Szűcs [a]

[a] Institute of Environmental Management, Faculty of Earth Science, University of Miskolc, 3515, Miskolc, Egyetemváros, Hungary
[b] Geology Department, Faculty of Science, Beni-Suef University, Beni-Suef, 65211, Egypt
[c] Department of Mineralogy and Geology, University of Debrecen, 4032 Debrecen, Hungary
[d] Department of Geology, Tanta University, 31527, Tanta, Egypt
[e] Division of Water Resources and Arid Land, Department of Hydrogeochemistry, Desert Research Center, Cairo, Egypt
[f] Center for Water Supply Studies, Texas A&M University-Corpus Christi, Corpus Christi, TX, 78412, USA
[g] Faculty of Earth Science, Beni-Suef University, 62511, Egypt
[h] Department of Earth and Ocean Sciences, University of North Carolina Wilmington, 601 South College Road, Wilmington, NC, 28403-5944, USA
[i] Geology Department, Faculty of Science, Tanta University, Tanta, 31527, Egypt
[j] Industrial Engineering Department, College of Engineering, King Saud University, P.O. Box 800, Riyadh, 11421, Saudi Arabia

ARTICLE INFO

Keywords:
Siwa oasis
Soil salinization
water quality deterioration
Hydrodynamic condition
Hydrochemistry
Geochemical modeling

ABSTRACT

The current study integrates remote sensing, machine learning, and physicochemical parameters to detect hydrodynamic conditions and groundwater quality deterioration in non-rechargeable aquifer systems. Fifty-two water samples were collected from all water resources in Siwa Oasis and analyzed for physical (pH, T°C, EC, and TDS) chemical (SO_4^{2-}, HCO_3^-, NO_3^-, Cl^-, CO_3^{2-}, SiO_2, Mg^{2+}, Na^+, Ca^{2+}, and K^+), and trace metals (AL, Fe, Sr, Ba, B, and Mn). A digital elevation model supported by machine learning was used to predict the change in the land cover (surface lake area, soil salinity, and water logging) and its effect on water quality deterioration. The groundwater circulation and interaction between the deep aquifer (NSSA) and shallow aquifer (TCA) were detected from the pressure-depth profile of 27 production wells penetrating NSSA. The chemical facies evolution in the aquifer systems were (Ca–Mg–HCO_3) in the first stage (freshwater of NSSA) and changed to (Na–Cl) type in the last stage (brackish water of TCA and springs). Support vector machine successfully predicted the rapid increase of the hypersaline lake area from 22.6 km^2 to 60.6 km^2 within 30 years, which deteriorated a large part of the cultivated land, reflecting the environmental risk of over-extraction of water for irrigation of agricultural land by flooding technique and lack of suitable drainage network. The waterlogging in the study was due

* Corresponding author. Institute of Environmental Management, Faculty of Earth Science, University of Miskolc, 3515, Miskolc, Egyetemváros, Hungary.

E-mail addresses: mohamedhamdy@science.bsu.edu.eg (M.H. Eid), ali.shebl@science.tanta.edu.eg (A. Shebl), mustafa.eissa@drc.gov.eg (M. Eissa), hassaan69@yahoo.com (E.A. Mohamed), amr_shaban@science.tanta.edu.eg (A.S. Fahil), hatem.bakry@science.bsu.edu.eg (H.S. Ramadan), aelsherbeeny@ksu.edu.sa (A.M. El-Sherbeeny), attila.geo.kovacs@gmail.com (A. Kovacs), hgszucs@uni-miskolc.hu (P. Szűcs).

https://doi.org/10.1016/j.heliyon.2024.e32992
Received 11 April 2024; Received in revised form 9 June 2024; Accepted 12 June 2024
Available online 15 June 2024

to a reduction in the infiltration rate (low permeability) of the soil and quaternary aquifer. The cause of this issue could be a complete saturation of agricultural water with chrysotile, calcite, talc, dolomite, gibbsite, chlorite, Ca-montmorillonite, illite, hematite, kaolinite and K-mica (saturation index >1), giving the chance of these minerals to precipitate in the pore spaces of the soil and decrease the infiltration rate. The NSSA is appropriate for irrigation, whereas TCA is inappropriate due to potential salinity and magnesium risks. The best way to manage water resources in Siwa Oasis could be to use underground drip irrigation and combine water with TCA and NSSA.

1. Introduction

The world is experiencing an extreme water shortage due to a lack of water supplies and deteriorating water quality. This issue will likely worsen in dry, densely populated areas and will have a crucial impact on agriculture in the future. To ensure sustainable agriculture, a holistic approach to managing soil, water, and crops will be necessary [1–8]. This approach will require tailored preventive measures and management strategies specific to each site and situation. Another challenge related to declining water quality is the problem of soil salinization [7,9–11]. Maintaining a careful balance between water and salt is crucial for stabilizing oasis-desert ecosystems that rely on groundwater in salt-affected areas. This is especially important in light of human development activities that can upset the delicate balance and climate variability that can threaten the sustainability of these systems [12–15]. In recent years, Egypt has directed considerable attention to expanding its agricultural projects utilizing groundwater resources, particularly in the western region of the Nile Delta and the New Valley, including Siwa Oasis, due to their soil and groundwater potential. Siwa Oasis relies solely on groundwater as its irrigation and drinking water source [7,9,16] as noted by Waterlogging, which refers to the continuous rise in the water table, is the most pressing issue faced by the Siwa Oasis, leading to a decline in the fertility of the soil due to soil salinization. This phenomenon is mainly attributed to poor management and over-irrigation practices in agriculture and inadequate drainage systems [7,9]. Over-irrigation has increased the surface area of salt lakes and soil salinity [17]. The surface lake area and groundwater salinity increased in different locations within Siwa Oasis, resulting in excessive deterioration of water quality, rendering it unsuitable for irrigation purposes [7,18].

Surface investigations are considered to be crucial for understanding subsurface conditions. Additionally, the combined use of remote sensing data, Geographic Information Systems (GIS), and machine learning has proven to be a cost-effective and robust method for monitoring soil salinization in closed sensitive ecosystems, as demonstrated by previous studies [11,19]. Thus, improving the evaluation of the environmental concerns regarding Siwa Oasis (e.g., soil salinity, water logging, groundwater salinization, and changes in land cover and surface salt lakes) requires adequate monitoring of the surface conditions mainly represented by the exposed land use/land covers. Consequently, it is essential to create reasonable thematic maps to identify LC/LU changes and comprehend them based on the data collected in the field and our geochemical investigations.

The hydrodynamic characteristics of confined sedimentary basins can be described under pressure or overpressure caused by geological processes like deposition, erosion, and tectonic compression [20,21]. These abnormal pressure conditions persist over geological time due to changing geological factors. The overpressure in groundwater flow systems creates excess perpendicular pressure that prevents vertical leakage from top layers, leading to non-renewable fluids due to geologically prevailing overpressure conditions [22]. Delineating the boundary between overpressure and gravity-driven systems is crucial for assessing water availability for drinking and irrigational utilization. While gravity-driven groundwater is regionally renewable on human and geological timescales, the overpressure zone is a closed system, and its water content cannot be replenished by precipitation, necessitating reinjection [23,24].

Groundwater quality changes result from natural processes, such as ion exchange, sorption, dissolution, precipitation of soluble minerals, acid-base reactions, oxidation-reduction reactions, evapotranspiration, and weathering of minerals [7,9,10,13,16,25–34]. Total dissolved solids, salinity, chlorinity, etc, reflect the overall concentration of solutes in groundwater at a particular time. It is related to the saturation states of the water samples [35]. Geochemical modeling tools like WATEQF, SOLMNEQ, and PHREEQC can calculate the saturation state of minerals in water to determine if a water sample has the potential to dissolve or precipitate minerals. The precipitation of some minerals in the agricultural soil can reduce its porosity, permeability, and rate of infiltration rate [36–38].

The sustainability of irrigation water quality has become an increasingly significant area of research worldwide. Several research studies have focused on developing hydrochemical indices to assess irrigation water quality comprehensively [39,40]. Among these indices, the Sodium Absorption Ratio (SAR), Sodium percentage (Na%), Magnesium Hazard (MH), Permeability Index (PS), and Residual Sodium Carbonate (RSC) are widely applied [31–33,41–44].

1. The aim of the study is environmental risk assessment through (1) change detection of the surface area of the salt lakes, water logging, cultivated land, and soil salinization in the period from 1990 to 2020 by using remote sensing, GIS, and machine learning, (2) detecting the effect of excessive abstraction of groundwater on aquifer pressure and hydrodynamic condition in the NSSA to detect groundwater flow and its vertical component, (3) application of geochemical modeling using PHREEQC to determine the mineral saturation state and its effect on the soil properties and human health, (4) irrigation water quality assessment and groundwater salinity monitoring from 1998 to 2022, (5) water management by using subsurface drip irrigation, perforated pipes, and mixing of water from TCA and NSSA to decrease groundwater quality deterioration and soil salinization.

2. Site description

Siwa Oasis is a closed depression situated in the northwestern desert of Egypt (Fig. 1). The Oasis fell within latitude and longitude 29°12′N and 25°43′E. The principal activity in the Siwa area is agriculture and industry [45]. The total area of Siwa Oasis is approximately 1100 km^2, with a population of 23546 residents. A severely arid climate characterizes Siwa Oasis [46]. The evaporation rate in summer is 16.8 mm/d, while in winter, it is about 5.4 mm/d. Rainfall in the Siwa area is negligible, with an annual precipitation of about 10 mm [47].

2.1. Hydrogeology

The exposed rocks in the depression of the Oasis are divided into several stratigraphic layers. The Quaternary deposits consist of sand dunes, sabkhas, clay, and silts. The Middle Eocene comprises limestone intercalated with shale [48]. Fig. 2a and b shows the surface geology and cross-section of Siwa Oasis. Siwa depression's hydrogeological setting includes five aquifers arranged from top to base, as follows: Quaternary deposits (shallow aquifer), Miocene, Eocene, Upper Cretaceous (carbonate aquifer), and Nubian sandstone aquifer (lower Cretaceous) [49,50]. Fig. 2b demonstrate a Hydrostratigraphic conceptual model and sequence stratigraphy of the study area.

The Miocene aquifer, located below the Quaternary aquifer and consists of fractured limestone, is the main aquifer in Siwa Oasis and is used for irrigation. Approximately 100 million m3 of water is discharged or removed annually from such aquifers [31,32]. The Nubian Aquifer (NSSA) contains high-quality water appropriate for irrigation and drinking, with depths ranging from 950 m to 1200 m BGL [50,51]. Recently, Siwa Oasis has faced severe problems such as soil salinization and waterlogging. The major lakes in the flat depression are Zeitoun, Aghormi, Siwa, and Maraqi lakes, arranged east to west (Fig. 2). These salt lakes receive water from different sources, such as drainage water from agricultural land, dug wells, and springs [52].

3. Material and methods

3.1. Remote sensing

Towards consistent thematic mapping over time series (30 years), four cloud-free Landsat scenes were collected in the same season. Three Landsat Five or thematic mapper (TM) images were implemented in 1990, 2000, and 2010, while the Landsat 8 or operational land imager (OLI) scene was adopted in 2020. These datasets (4 scenes) were obtained from the US Geological Survey (USGS). Theircharacteristics, including the spectral and spatial attributes of the two utilized sensors (TM and OLI), were reported (Table 1s).

Due to the considerable change within the study area, it is a tedious task to create a traditional LU/LC mapping. Thus, objective mapping using the power of machine learning algorithms is introduced in the current research using the well-known support vector machine (SVM) algorithm [56]. In the current study, image processing techniques represented by false color combinations constituted one of the best data inputs that discriminate most of the exposed features within the study area. Thus, and to be more consistent, false color composites representing the same spectral ranges for the four scenes were selected for visual interpretation, comparing LU/LC changes. For instance, FCC 7 (Short-wave Infrared) −4 (Near Infrared) - 2(green) in RGB respectively was utilized with Landsat TM data, and relatively similar spectral regions were utilized with Landsat OLI data represented by FCC 7 (Short-wave Infrared) −5 (Near Infrared) −2 (blue) in RGB respectively. These FCCs were adopted as a reference map for extracting training and testing data concerning previous maps and our field investigations. Six classes, including lake water, shallow water (wet sabkha), marshes (dry

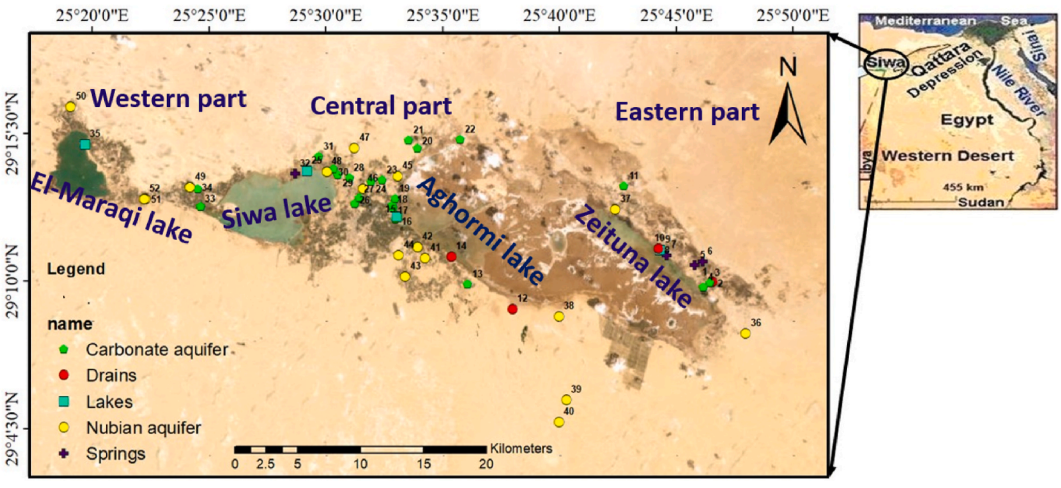

Fig. 1. Distribution map of the sampling points from all water resources in the study region.

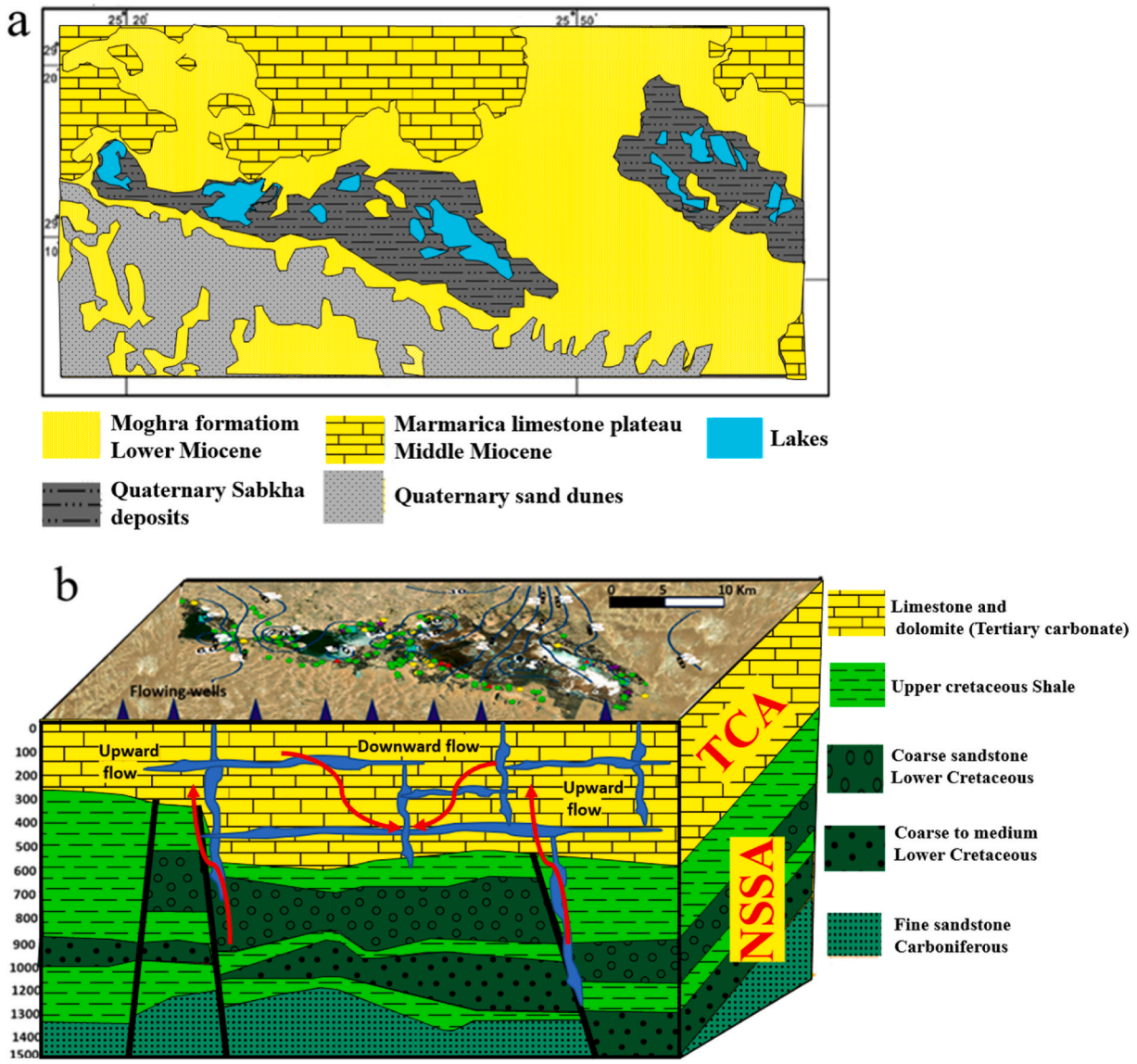

Fig. 2. Geological map (a) and Hydrostratigraphic conceptual model of the Oasis (b).

Table 1
The computation methodology of the irrigation indices.

IWQIs	Formula	References
SAR	$\left(\frac{Na^{+}}{\sqrt{(Ca^{2+}+Mg^{2+})/2}}\right)\times 100$	[[53]
Na %	$\frac{(Na^{+}+K^{+})}{(Ca^{2+}+Mg^{2+})+(Na^{+}+K^{+})}\times 100$	[[53]
MH	$[Mg^{2+}/(Mg^{2+}+Ca^{2+})]$ *100	[54]
PS	$Cl^{-}+\left(\frac{SO_4^{2-}}{2}\right)$	[55]
RSC	$(HCO_3^{-}+CO_3^{-})-(Ca^{2+}+Mg^{2+})$	[53]

The IWQIs are determined in meq/L.

sabkha), cultivated land, Moghra formation, and sand dunes, were outlined after visual overlay analysis of the previously mentioned FCCs and georeferenced previous maps. Towards unbiased classifications, training and testing data were kept spatially constant (from the same locations) throughout the whole process. Table 2s summarizes the characteristics of training and testing data. As recommended by several researchers [56–58]The percentages of training and testing data are kept between 70 – 80 % and 30–20 %, respectively. These training pixels are used to train the classifier over the four main data inputs (the whole number of bands for Landsat TM and OLI).

3.2. Machine learning model (SVM)

SVM essentially relies on fitting a separating hyperplane that, given a multidimensional feature space, offers the optimum separation between classes [59].The decision surface on which the ideal class separation occurs describes this hyperplane. The classifier's generalization error is often smaller with the wider the margin (separating the training data). Therefore, the hyperplane is only constructed using the support vectors, a subset of the training samples, offering wider margin and maximum separation. The current research adopted RBF as a kernel due to its well-reported results from several previous similar studies [58,60,61]. Additionally, and concerning previous literature, the algorithm is also given a penalty parameter (was assigned as 100) to account for misclassification during training.

3.3. Hydrodynamic data and method of calculations

To investigate the water pressure of the NSSA and hydrodynamic conditions in Siwa Oasis, the pressure head, screen depth interval, ground surface level, water temperature, density, and elevation head were measured in 27 wells (Table 2). The hydraulic head is proportional to the fluid potential (ϕ) in a given point of rock framework and represents the amount of mechanical energy contained by a unit mass of incompressible fluid, as shown in equation (1) [22,62]. The pressure (P) was determined using Equation (2). Elevation head (Z) is equal to the difference between total head (h) and pressure head (Ψ) (equation (3)), where pressure head (Ψ) is the difference between total head (h) and elevation head (Z) (equation (4)).

$$\phi = g.z + p/\rho = g/h \tag{1}$$

$$P = (h - z) \times \rho \times g \tag{2}$$

Table 2
The input data used for the calculation of aquifer pressure in Siwa Oasis.

Samples	Water level asl (hw)	Ground level (GL)	Screen depth (S)	Temperature (T)	Density (ρ)	Elevation head (Z)	Pressure head (Ψ)	Total head (h)	Pressure (P)
37	87	−1987	−950	40	992.17	1037	1050	2087	10209429.3
46	6.27	−1985	−900	40	992.17	1085	921.27	2006.27	8957753.27
49	8.18	−1994	−835.425	40	992.17	1158.575	849.605	2008.18	8260935.41
45	14.79	−1990	−808.45	37.9	992.93	1181.55	833.24	2014.79	8108020.13
P1	14.82	−1990	−812	41.2	991.78	1178	836.82	2014.82	8133425.13
42	29.46	−1994	−841.225	41.5	991.78	1152.775	876.685	2029.46	8520890.76
P2	30	−2022.5	−656.14	37.8	993.28	1366.36	663.64	2030	6459967.32
47	31.27	−2010	−779	40.5	992.17	1231	800.27	2031.27	7781238.08
52	33.8	−1993	−827	35.5	994.98	1166	867.8	2033.8	8461747.71
P3	36.24	−1990	−764.21	40.5	992.17	1225.79	810.45	2036.24	7880220.93
P4	43.67	−1987.1	−745	37.8	993.28	1242.15	801.52	2043.67	7802111.1
44	52.6	−1991	−922.5	38.5	992.93	1068.5	984.1	2052.6	9575995.65
51	53	−1993	−691.635	37.5	993.28	1301.365	751.635	2053	7316523.33
41	53.6	−1992	−745	37.8	993.28	1247	806.6	2053.6	7851560.55
P5	55.5	−1988	−721.97	41.2	991.78	1266.03	789.47	2055.5	7673209.45
48	55.6	−1994	−762.1	39.5	992.55	1231.9	823.7	2055.6	8012121.66
43	56.6	−1995	−793.5	39.7	992.55	1201.5	855.1	2056.6	8317549.15
P6	57	−1991.7	−764.21	39	992.55	1227.51	829.49	2057	8068440.94
40	58.17	−2044	−920	39	992.55	1124	934.17	2058.17	9086662.25
39	66.38	−2038	−1037.5	41.8	991.39	1000.5	1065.88	2066.38	10355687.2
50	75	−1991.5	−810.59	37.2	993.28	1180.91	894.09	2075	8703200.81
P7	85	−1990	−899.4	40	992.17	1090.6	994.4	2085	9668815.71
38	87.5	−1985	−843.355	38.1	992.93	1141.645	945.855	2087.5	9203844.49
P8	94	−1989	−790	43	991.78	1199	895	2094	8698902.38
36	95	−1991.1	−896.04	41.5	990.99	1095.14	999.86	2095	9710342.36
P9	97.5	−1994.5	−945.42	39	992.55	1049.08	1048.42	2097.5	10197970.9
P10	110	−1999	−927.58	37.9	992.93	1071.42	1038.58	2110	10106124.9

The pressure head fell between 663.6 m and 1065.8. The calculated water pressure in NSSA has a minimum value of 6459967 Pa and a maximum value of 10355687 Pa. The following results are based on the combined interpretation of p(z) profiles (Fig. 5b), a water potential map (Fig. 5c), and the conversion of water level to pressure (Fig. 5d).

$$Z = h - \Psi \tag{3}$$

$$\Psi = h - Z \tag{4}$$

Equation (2) can be used to convert pore pressure (p) and hydraulic head (h) data to one another (Fig. 5a), where z denotes the elevation of the midpoint of the screened depth ranges in the water boreholes, and h and P are the observed values.3.4 Hydrogeochemical characteristics.

3.4. Groundwater sampling and laboratory analyses

In February 2022, 52 samples were collected from surface and groundwater samples, and various field measurements were performed. The collected water samples were analyzed for chemical composition at the Desert Research Center (DRC) laboratory in Cairo, Egypt. Portable pH and EC meters were used to measure pH and EC in the field and laboratory immediately after sampling. Groundwater was collected in polyethylene bottles and subsequently tested for primary ions. (Ca^{2+}, Mg^{2+}, Na^{+}, K^{+}, HCO_3^{-}, CO_3^{2-}, SO_4^{2-}, Cl^{-}) in the laboratory. A flame photometer (Jenway PFP 7) was used to determine Na^{+} and K^{+}, while standard EDTA procedures were used for titrimetric determination of total hardness (TH), $CaCO_3$, and Ca^{2+}. Volumetric methods were used to analyze CO_3^{2-} and HCO_3^{-}, and Mg^{2+} was calculated from the TH and Ca^{2+} contents. Chloride ion was estimated using $AgNO_3$ (titration method), while sulfate was determined using turbidity. The levels of heavy and trace metals were determined using ICP. The analytical precision of the measurements of cations and anions was calculated from the ionic balance error (IBE). The value of IBE did not exceed ±5 %. The Ionic Balance (IB) is a percentage difference in water's overall concentration of cations and anions (Equation (5)). TC represents total cations, and TA represents total anions in milliequivalents per liter.

$$\%IBE = ((TC–TA) / (TC + TA)) \times 100 \tag{5}$$

3.5. Geochemical software

DIAGRAMMES software and Excel sheets were used to develop the Piper diagram, Chadha diagram, and irrigation indices for hydrogeochemical evaluation of surface and groundwater. PHREEQC software models the net geochemical mass-balance reaction among initial and final waters according to a hydrologic flow path. The amount of reactants (in mmol/kg of H2O) that dissolve in the various water samples and the number of products precipitated from the resulting solution were estimated. The saturation indicator (SI) is positive when a solution is over-saturated, negative when it is subsaturated, and zero at balance [41–44]. Equation (6) was used

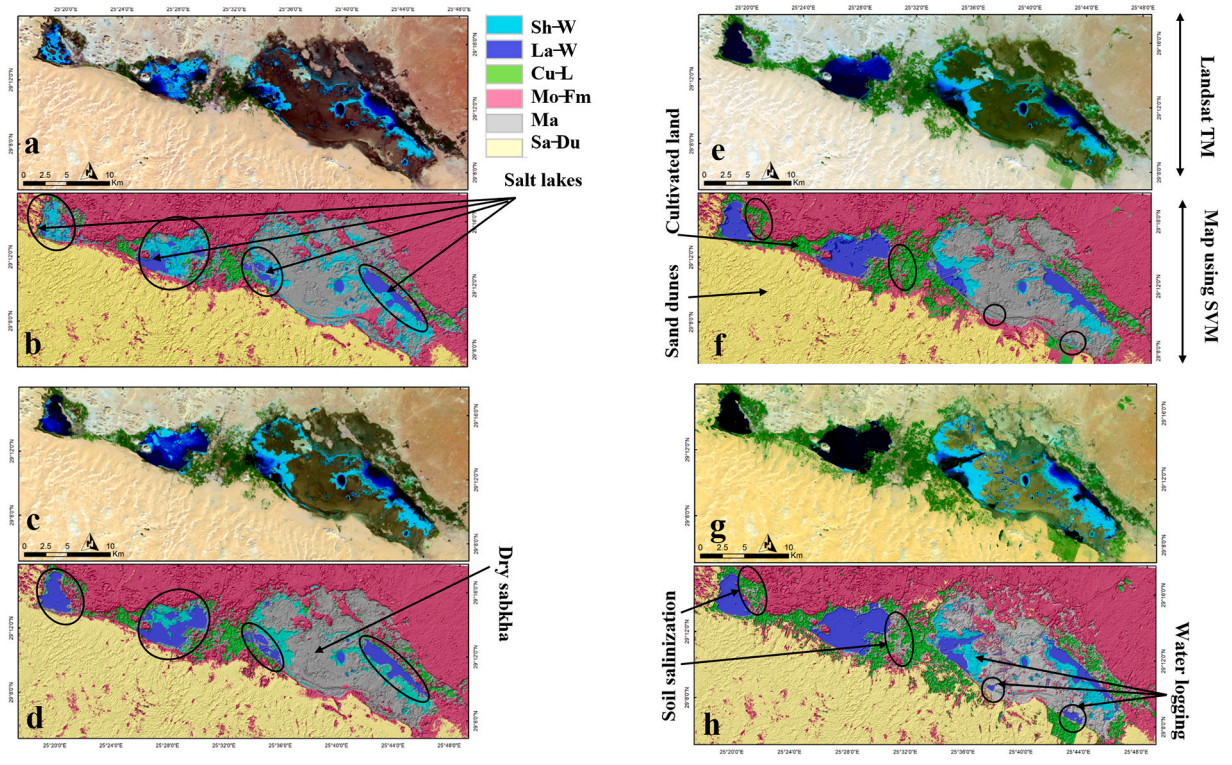

Fig. 3. FCC 7-4-2 in RGB respectively for Landsat TM a) 1990, c) 2000, e) 2010, g) OLI 2020 and their corresponding resultant thematic map using SVM (b, d, f, and h respectively).

to compute the saturation state.

$$\Omega = IAP/K \tag{6}$$

Where IAP is the ion activity product and K is the solubility product. If $\Omega < 1$, the subsaturating state prevails, while $\Omega > 1$ indicates that the supersaturating state prevails. The saturation index (SI) is given by equation (7);

$$SI = log\frac{IAP}{K} \tag{7}$$

At SI = 0, the constituent minerals and solution are in equilibrium. A negative SI level indicates a sub-saturated state, whereas a positive SI level indicates a supersaturating state, which causes precipitation and renders the solution unsuitable for dissolving minerals.

3.6. Irrigation indices (IWQIs) and water quality

The five irrigation indices (Table 1) were calculated using the chemical parameters.

4. Result and discussion

4.1. Change detection with remote sensing data and support vector machine

Through analyzing the spectral characteristics of the exposed targets within the study area, it was found that the best band combinations that significantly contribute to their discrimination are 7-4-2 in RGB respectively for Landsat TM and 7-5-2 in RGB respectively for Landsat 8 (Fig. 3). These color composites provide a natural-like performance that is easily differentiated. The FCCs, band 7 (2.08–2.35 μm) could sharply separate water (strong absorption) from land (strong reflectance) and help identify four main land covers within the study area (shallow water, lake water, Moghra formation, and sand dunes). Band 4 (0.76–0.90 μm) is an essential channel as it provides the best spectral range for vegetation (higher NIR reflectance) differentiation (green color). Water is delineated by its NIR strong absorption (depending on the water depth), and barren lands and urban areas are primarily highlighted in darker tones. Band 2 (0.52–0.60 μm) is picked out as a third band in our informative combination as it could provide some kind of

Table 3
Descriptive results of the physical parameters, chemical parameters, and heavy metals in surface and groundwater samples.

Type	Value	pH	T°C	EC (μS/cm)	TDS (mg/L)	TH (mg/L)	Ca^{2+} (mg/L)	Mg^{2+} (mg/L)	Na^{+} (mg/L)	K^{+} (mg/L)	Cl^{-} (mg/L)
NSSA	min	6.4	35.5	268	160	63.7	9.8	2.3	18	13	40.6
	max	8.8	41.8	642	489	265.05	64.7	56.5	100	23	156.6
	average	8	39.1	404	286	133.9	24.5	19.0	46	19	90.1
TCA	min	7.47	17.7	7450	6306	1715	98.0	83.3	1016	4	3364
	max	8.45	27.7	24250	17880	11160	1116	2033.9	4600	83	11368
	average	7.8	24.2	11384.4	8843	3884.5	475.6	644	1876	59	5238.6
Springs	min	7.6	24	8450	6499	1674	297.6	113.0	1400	49	3654.0
	max	7.98	25.1	11790	8885	3887.4	1264.8	583.1	1845	77	5220.0
	average	7.7	24.5	10561.6	7680	2892.3	691.3	331.8	1668	67	4403.2
Drains	min	7.89	18.8	9180	7306	3255	568.4	406.8	1240	5	4060
	max	8.6	20.9	20490	16126	6370	1568.0	888.3	3750	83	9744
	average	8.2	20.1	13776.7	10858	4924.9	969.8	650.0	2138	42	6191.5
Lakes	min	7.83	17.5	108400	84835	23324	1568.0	4715.2	23750	10	52200
	max	8.36	27.1	188800	153589	55664	2508.8	12216.6	39500	18	94250
	average	8.15	21.6	150366.7	118895	38089.3	2064.5	8037.2	32042	14	72983.3

Type	**Value**	**SO_4^{2-}** (mg/L)	**HCO_3^-** (mg/L)	**NO_3** (mg/L)	**SiO_2** (mg/L)	**Fe** (mg/L)	**Mn** (mg/L)	**Sr** (mg/L)	**B** (mg/L)	**Ba** (mg/L)	**Al** (mg/L)
NSSA	min	1.6	89.7	1.4	2.9	1.25	0.02	0.04	**0.06**	0.1	0.1
	max	73.1	185.3	18.2	19.7	27.65	0.9	0.28	4.4	0.41	23.9
	average	19.7	137.2	5.2	10.8	3.15	0.19	0.11	0.6	0.14	2.0
TCA	min	85.3	89.7	2.8	0.2	0.4	0.01	2.475	0.1	0.01	0.002
	max	992	197.3	29.4	19.3	6.07	0.16	12.35	1.6	0.09	0.561
	average	494.9	166.2	8.6	7.8	0.5	0.06	7.2	1.0	0.05	0.21
Springs	min	302.9	167.4	6.3	5.2	0.03	0.01	5.97	0.4	0.01	0.1
	max	550.0	185.3	13.3	17.2	0.18	0.06	9.97	0.9	0.04	0.4
	average	449.2	175.4	9.2	12.8	0.12	0.03	8.25	0.6	0.02	0.2
Drains	min	500.0	125.5	1.4	11.5	0.01	0.005	5.8	0.6	0.03	0.1
	max	1850.0	269.0	4.2	18.9	2.07	0.029	16.2	0.7	0.05	0.3
	average	995.1	202.3	3.3	15.8	0.72	0.018	10.4	0.7	0.04	0.1
Lakes	min	2500.0	167.4	2.8	2.1	0.07	0.07	18.72	7.9	0.043	0.4
	max	5348.7	215.2	4.2	9.4	5.24	1.75	30.43	16.9	0.92	45.6
	average	3716.9	191.3	3.7	6.2	1.81	0.63	25.745	11.4	0.36	15.5

differentiation of water, based mainly on their turbidity level, and highlights barren lands and urban areas in lighter tones. The SVM classification results for these targets (six classes) are displayed (Fig. 3) and statistically assessed (Table 3s) through confusion matrices and kappa coefficients (k) as well-known measures for classifiers' performance and their resultant thematic maps.

4.1.1. Change detection in land cover

Spatio-temporal changes in different landcover classes, which were monitored in the whole area and surrounded the main four lakes (Table 4s and Fig. 3). The total area of the saltwater bodies (hypersaline lakes) was estimated at 22.6, 42.6, 53.1, and 60.6 km^2 in 1990, 2000, 2010, and 2020, respectively. Siwa Lake is the largest lake (29 km^2) and Aghormi (6.6 km2) is the smallest. The increase in surface area is more pronounced concerning the El Maraqi, Siwa, and Aghormi lakes while there is more or less a natural balance for the Zeituna lake due to evaporation rate nearly equal the inflow rate to the lake or there is seepage from Zeituna lake to the shallow aquifer.

The findings showed that the surface area of salt lakes increased rapidly from 1990 to 2020, except for the period between 2010 and 2020 when Zeituna Lake's surface area dropped. The substantial increase in the surface area of Siwa, Aghormi, and El Maraqi Lakes reflects the effect of access discharge from TCA and NSSA for reclamation of new agricultural lands (Fig. 3).

The decrease in Zeituna Lake surface area from 2010 to 2020 was due to an improved irrigation and drainage system, and the closure of the poor wells, which contributed to a decreased surface area for the Zeituna Lake [50]. Expanding the surface area of saltwater lakes is closely related to increasing the cultivated land area, which requires additional pumping wells and agricultural drainage discharging into the lakes. It was estimated that the cultivated area in Siwa Oasis is 23.9, 34.5, 82.5, and 89 km^2 in 1990, 2000, 2010, and 2020, respectively, showing an increase in the reclamation of new agricultural land, especially in the central part of the Oasis. The surface area of the shallow water (wet sabkha) close to the four lakes decreased from 80.2 to 25.3 km^2 from 1990 to 2010, when a large area changed to dry sabkha due to evaporation. There was a slight increase in shallow water (wet sabkha) from 25.2 to 31.1 km2 from 2010 to 2020 due to new cultivated area and agricultural drainage extended between Aghormi and Zeituna lakes. The surface area of the dry sabkha or marches increased from 145.6 to 174 km^2 in the period from 1990 to 2000 due to the evaporation of shallow water or water logging area leaving behind dry sabkhas. The dry sabkha area started to decrease from 174 to 157.7, and 143.7 km^2 in 2000, 2010, and 2020. The area of sand dunes decreased with time due to reclamation of new areas for agriculture in the southern part of Siwa Oasis. In the period from 2010 to 2020, the land cover changed from cultivated area to dry sabkha as a result of evaporation of water logged in the soil leaving behind salinized soil in the entire study area specifically in the central study area. The water logging and soil salinization was detected through field observations (Fig. 4). The total area of dry sabkhas decreased due to an increase in the surface extent of lakes in the study area. a considerable extension of the dry sabkha was intense near the vegetation cover. A Significant land area became salinized during the period of 2010–2020. This indicates that the salinization rate has accelerated since 2010. Most of the depleted vegetation was located close to the saline lake waters, and the wet sabkha.

Increasing the surface area of the Siwa and El Maraqi lakes refers to excessive groundwater extraction, which causes a drop in water level (cone of depression). The over-abstraction of groundwater from the central part of Siwa Oasis can have a negative effect on the water pressure of the NSSA and decrease the vertical upward movement to recharge the TCA. The NSSA is limited and non-rechargeable, and it is the main source of fresh water in the Oasis. Increasing the dry sabkha or soil salinization and waterlogging over time reflects the poor irrigation water quality and deterioration of soil properties.

4.2. Hydrodynamic condition of the aquifer system

To investigate the water pressure of the NSSA and hydrodynamic conditions in Siwa Oasis, the pressure head, screen depth interval, ground surface level, water temperature, density, and elevation head were measured (Table 2). The screen depth interval ranges from

Table 4
Statistical analysis and classes of irrigation water quality indices.

Criteria	Min	Max	Mean	Range	Class	Number of Samples (%)
SAR	0.6	90.6	15.3	<10	Excellent	22(42.3 %)
				10–18	Good	21(40.4 %)
				19–26	Fair Poor	4(7.7 %)
				>26	Unsuitable	5(9.6 %)
Na%	24.5	71.3	51.4	<20 %	Excellent	0(0 %)
				21%–40 %	Good	10(19.2 %)
				41%–60 %	Permissible	29(55.8 %)
				61%–80 %	Doubtful	13(25 %)
				>80 %	Unsuitable	0(0 %)
MH	9.1	90.3	61.1	<50	Suitable	7 (13.5 %)
				>50	Unsuitable	45(86.5 %)
PS	1.3	2713.5	291.4	<3	Excellent to good	12(23.1 %)
				3–5	Good to injurious	5(9.6 %)
				>5.0	Injurious to unsatisfactory	35(67.3 %)
RCS	1109.5	1.3	−116.9	<1.25	Good	51(98.1 %)
				1.25–2.5	Doubtful	1(1.9 %)
				>2.5	Unsuitable	0(0 %)

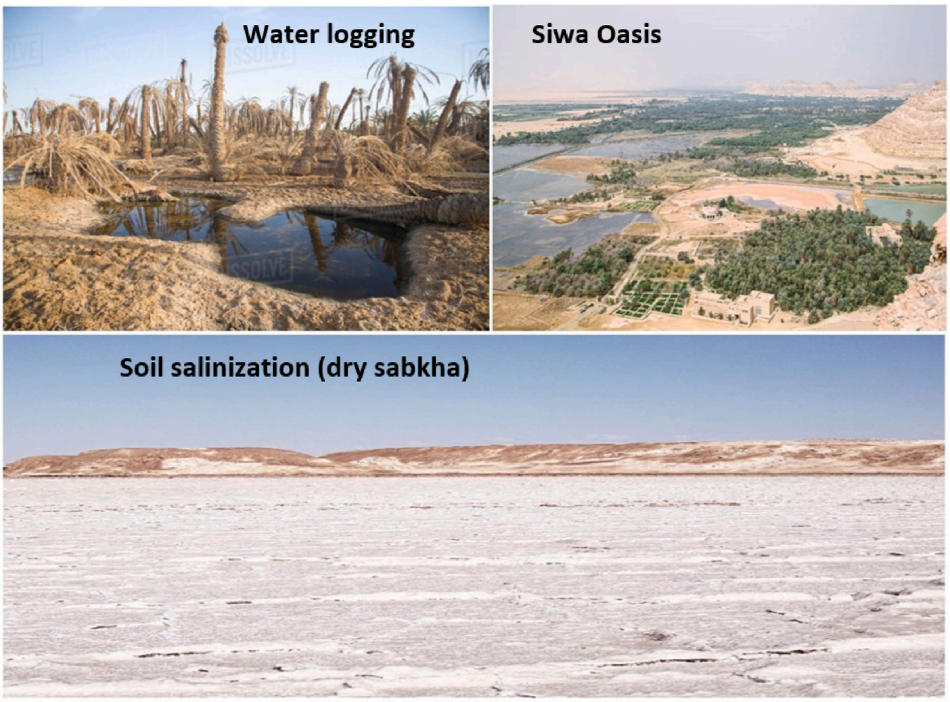

Fig. 4. Field observation of the water logging and soil salinization (dry sabkha).

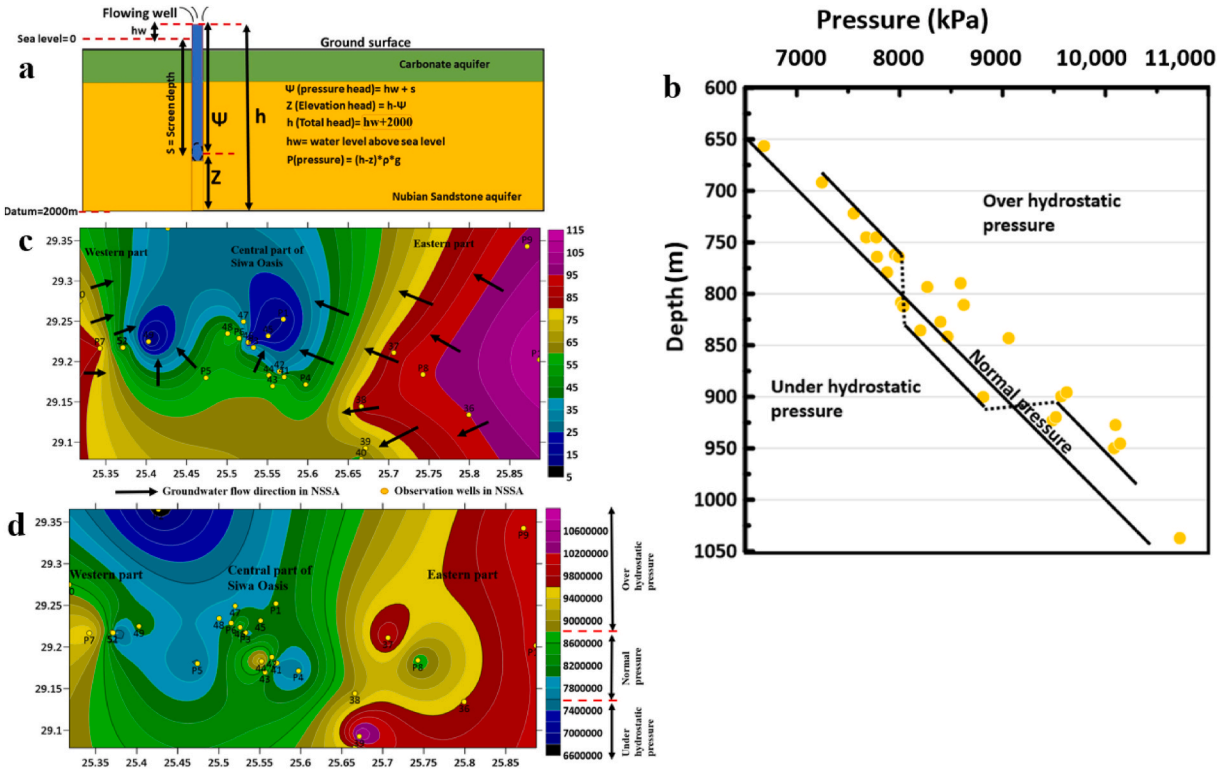

Fig. 5. (a) Schematic diagram for the calculation of the water pressure, (b) Pressure-depth profile, (c) Groundwater flow direction, and (d) Distribution map of the water pressure.

656.1 m to 1037.5 m below ground level. The water level above sea level had a minimum value of 6.3 m in the central part of Siwa Oasis and a maximum value of 110 m above sea level in the east part of Siwa Oasis, respectively.

The pressure raised with depth in the direction of the eastern and western parts of Siwa Oasis at a rate greater than hydrostatic pressure while decreasing in the central and northern parts to hydrostatic pressure. According to the Pressure-Depth curve, 18 samples fell above the hydrostatic line, indicating an over-hydrostatic pressure zone and upward groundwater movement. In comparison, three samples fell below the hydrostatic line, indicating that the water contained within the NSSA is under hydrostatic pressure and downward groundwater movement. The rest fell on the hydrostatic line, indicating that there is no vertical component of groundwater flow (Fig. 5b). Instead, horizontal groundwater flow dominates this zone. The local groundwater flow in Siwa Oasis has two directions: SE-NW from the eastern side of the research area and SW-NE from the western side (Fig. 5c). The eastern and western parts of the Siwa Oasis represent the recharge zone. In contrast, the middle and northern parts represent the discharge area. The central location of Siwa Oasis around Siwa lake showed cone of depression in the groundwater level, and the water pressure is under hydrostatic pressure. As mentioned before, Siwa Lake is the largest lake in the study area as it receives more water from the agricultural drainage. From these evidences, the water pressure in NSSA has dropped to be under hydrostatic pressure around Siwa lake due to over abstraction of groundwater in this location. In the current study the pressure gradient changes with distance in the confined aquifer (NSSA) giving indication of upward groundwater flow from NSSA to TCA through the fault plane. The result showed that the over abstraction of groundwater for drinking and irrigation could decrease the water pressure in the NSSA which has a risk on the limited water resources quality and quantity in Siwa Oasis and can be a sign of depletion of groundwater quantity in Nubian aquifer (non-rechargeable). The extensive irrigation in Siwa by flooding method could waste much water more than the needs of crop production and decrease the recharge of TCA from NSSA. Decreasing the upward movement of groundwater in the NSSA could decrease the recharge of the TCA by fresh water from the NSSA, hence decreasing its water pressure. If the pressure in the TCA decreased under hydrostatic pressure, it would promote downward movement of groundwater, which could raise the diffusion of salt water from the surface lakes and drains,

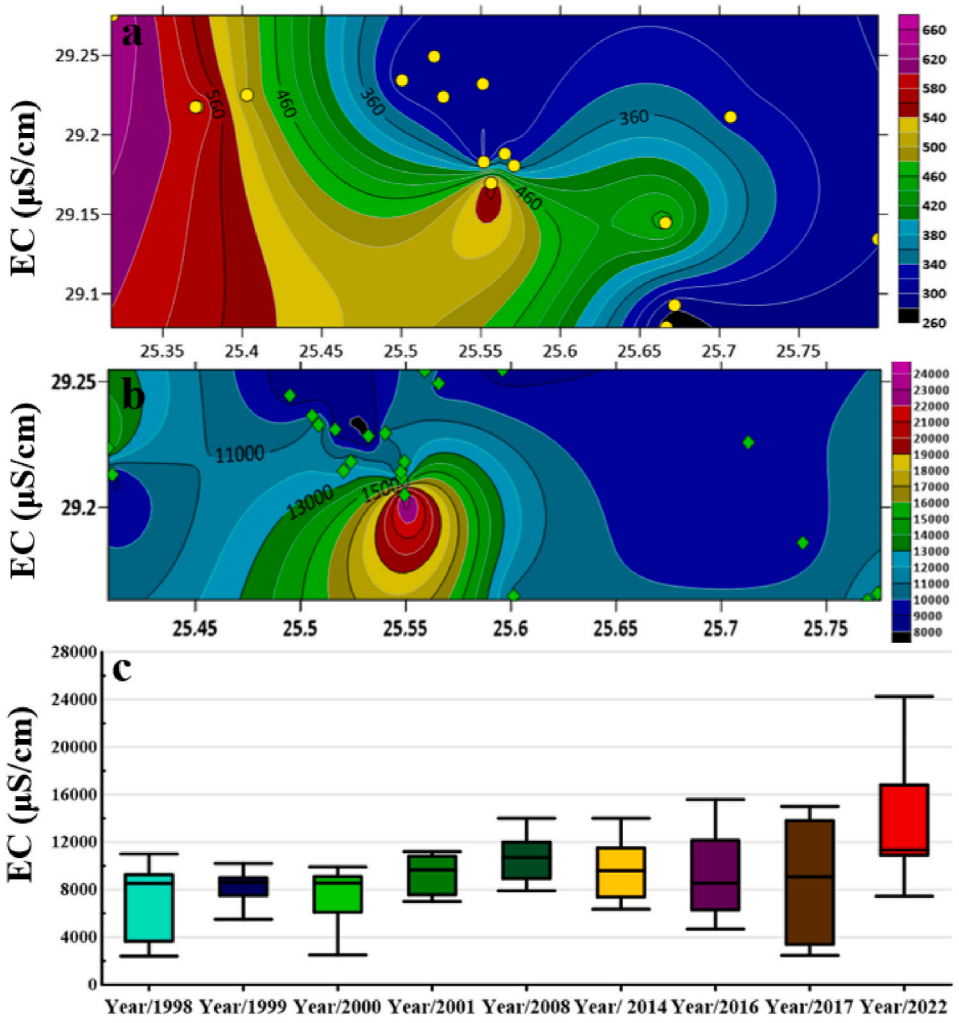

Fig. 6. Distribution map of EC in NSSA (a), TCA (b), and Box plot of the EC in TCA from 1998 to 2022 (c).

seep downward, and deteriorate shallower and deeper aquifers. Increasing the groundwater salinity in the TCA is the main reason for the soil salinization. The water pressure decreased in the central and northern parts of Siwa Lake under hydrostatic pressure (Fig. 5d), and the soil salinization increased in the same area from 2010 to 2020 (Fig. 3f–h), which confirms the current interpretation.

4.3. Hydrogeochemical and monitoring processes

The quality of the surface and groundwater was evaluated using physicochemical parameters, trace elements, and heavy metals. The results, including the minimum, maximum, and average values of the surface water and groundwater, are presented in Table 3.

The average temperature of the water samples in the deep aquifer (NSSA), shallow aquifer (TCA), springs, drains, and lakes was 39.1 °C, 24.2 °C, 24.5 °C, 20.1 °C, and 21.6 °C respectively. The pH averages 8, 7.8, 7.7, 8.2, and 8.15 for the Nubian, tertiary aquifers, springs, drains, and lakes, referring to the neutral to slightly alkaline conditions of the surface water and groundwater in Siwa Oasis. The total dissolved solids (TDS) mean value was 286, 8843, 7680, 10858, and 118895 mg/L in the in Nubian and tertiary aquifers, lakes drain, and springs. It was reported that the water is fresh in NSSA, brackish in TCA and springs, saline in the drains, and

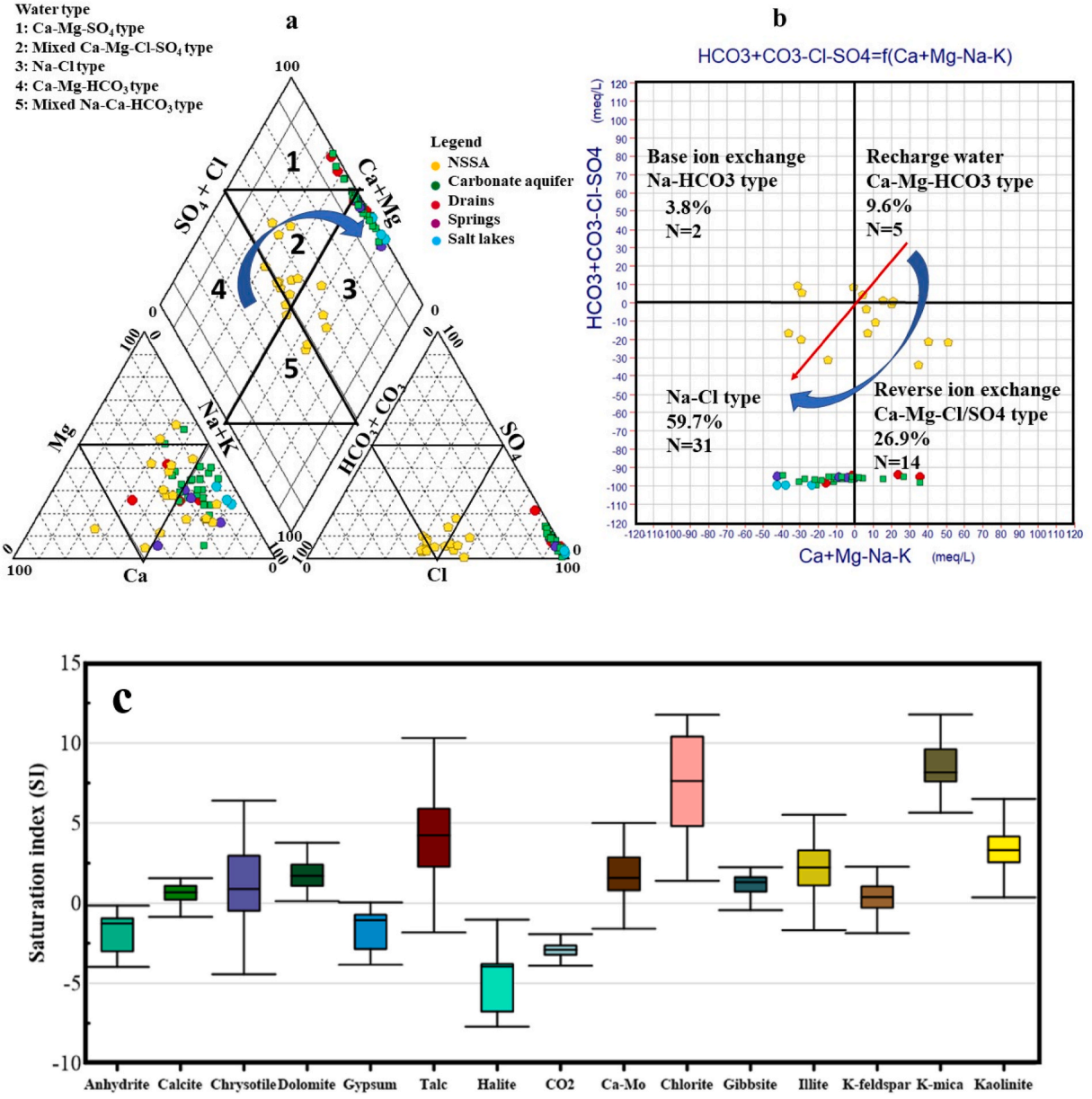

Fig. 7. Graphical representation of the water type and geochemical evolution, (a) Piper diagram, (b) Chadha diagram, and (c) Saturation index of minerals in the surface water and groundwater.

hypersaline in the lakes, which reveals that all the collected water samples are not suitable for drinking and irrigation except NSSA [63, 64]. The distribution map of the EC in the NSSA and TCA (Fig. 6a and b) revealed that the central area of Siwa Oasis is more vulnerable to water quality deterioration and soil salinization. A box plot was created to represent the history of the TCA's groundwater salinity and integrate the change detection of the cultivated land and water quality in the same period. Monitoring the salinity (EC) of the TCA from 1998 to 2022 showed rapid deterioration in the groundwater quality due to increasing water salinity (Fig. 6c). In 1998, the value of EC ranged from 2400 to 11000 with an average value of 6880 μS/cm, while in 2022, the value of EC fell between 7450 and 24250 with a mean value of 14425 μS/cm. This indicates that the water is not suitable for irrigation purposes. It was noted that water salinity increased rapidly from 2017 to 2022 compared to the period from 1998 to 2017, resulting from the reclamation of new agricultural areas and the pumping of more groundwater from TCA. The current water salinity of the TCA could deteriorate the soil properties and decrease plant production through salt accumulation.

The average value of the total hardness was 133.9, 3902, and 38089 in the NSSA, TCA, and surface water, respectively. The findings demonstrated that the tested water is soft to moderately hard in NSSA and very hard in TCA and surface water. The dissolution of minerals like calcite, dolomite, and gypsum minerals releases substantial amounts of Ca^{2+} and Mg^{2+} ions into the water, increasing the total hardness of the TCA.

The hydrochemical facies of the groundwater samples were categorized using a Piper plot [65] (Fig. 7a). The diamond-shaped plot classified the samples into four water types. six samples, including four samples of TCA, and two samples of drains belong to Ca–Mg–SO_4 water type (zone 1). The second groundwater category, the third zone (Na–Cl facies), consisted of 19 TCA sample, 3 NSSA sample, four Salt Lake samples, four spring samples, and two drain samples. The final two classes in zones two and five (mixed Ca–Mg–Cl–SO_4 and mixed Na–Ca–HCO_3 facies) represented the remaining NSSA samples. The salinity index (SO_4^{2-} + Cl^-) was higher than the alkalinity (HCO_3^- + CO_3^{2-}), and the alkalis (Na^++K^+) exceeded the alkaline earth (Ca^{2+} + Mg^{2+}), indicating the hydrochemistry of the Tertiary carbonate aquifer and NSSA in the study area. The relatively low bicarbonate content of groundwater suggested that annual recharge was low and that groundwater in the study area was a non-rechargeable resource. The most dominant geochemical mechanism that governs water chemistry was determined using the Chadha diagram [66] (Fig. 7b). Most of the samples (59.7 %) including salt lakes, springs, 2 samples of drains,17 samples from TCA, and only 3 samples from NSSA, were plotted in the field of Na–Cl type, which recommends replacement of Ca^{2+} and Mg^{2+} with Na^+ through ion exchange process and seepage from the hypersaline lakes and drains due to cone of depression in the water level and decline in the groundwater pressure. The three samples of NSSA (43, 49, and 51) with Na–Cl type are situated in the region where the water's pressure falls below hydrostatic pressure (Fig. 5d). This indicates that the vertical downward movement of the groundwater in NSSA due to excessive extraction could create a mixing zone between the water in TCA and NSSA. The water salinity (EC) of samples 43, 49, and 51 are 332, 583, and 642 mg/L, representing the highest values of EC in NSSA compared to the other samples, which indicates that the water quality in the NSSA will deteriorate with time from the shallow aquifer.

About 26.9 % of the water samples, including six samples of TCA, and two samples from the drains fell in the reverse ion exchange zone with Ca–Mg–Cl/SO4 water type, and two samples from NSSA fell within the base ion exchange zone with Na–HCO_3 water type. The remaining 9.6 % of the samples (NSSA samples) fell within the recharge water zone with water type Ca–Mg–HCO_3. Chadha's diagram showed that the water type changed upward from Ca–Mg–HCO3 in the first stage in the deep aquifer (NSSA) to the Na–Cl type in the last stage in the shallow aquifer (TCA) and surface water.

4.4. Geochemical simulation and modeling

The current investigation computed minerals or salts in the investigated water and determined the minerals that might precipitate in soils, reducing permeability and causing water logging. The PHREEQC models were utilized in this research to examine the mineral accumulations and saturation conditions of significant minerals in every water source in Siwa Oasis, using input parameters including physical, chemical, and trace elements (Table 3). saturation levels (SI) were determined for Ca-montmorillonite, calcite, kaolinite, K-mica, gypsum, dolomite, talc, potassium feldspar, chrysotile, chlorite, gibbsite, hematite, anhydrite, and illite. Deposing minerals like these in soil over time can reduce porosity and infiltration rate, resulting in waterlogged and dry sabkha following shallow water evaporation. The model also provided the partial pressure of carbon dioxide (CO_2) (Fig. 7c), and it was depleted with a value less than zero, indicating a decrease in the replenishment quantity of the aquifers. The NSSA's samples exhibited a salt combinations assemblage consisting of NaCl, Na_2SO_4, $NaHCO_3$, Ca (HCO3)2, and Mg (HCO3)2, as a consequence of leaching, or terrestrial salt dissolution, and ion exchange. The cation exchange mechanisms increased the concentration of Na + while lowering the concentrations of magnesium and calcium in the solution, resulting in a considerable rise in water salinity. Furthermore, the loss of magnesium and calcium decreased the water saturation level for calcite, anhydrite, gypsum, and dolomite minerals. The saturation statuses for essential minerals revealed that all investigated samples were under-saturated in terms of anhydrite, gypsum, and halite, indicating that the groundwater can dissolve substantially more of these minerals, increasing water salinity.

In almost all samples, the SI of chlorite, hematite, kaolinite, and K-mica was positive (supersaturation condition). A significant number of samples were found to be over-saturated (Saturation index >0) about talc, illite, chrysotile, dolomite, gibbsite, potassium feldspar, Ca-montmorillonite, and calcite, with minimum values of −6.6, −1.6, −9.1, −513,-0.45, −1.8, −2.7, and −257, and maximum values of 11.8, 9.5, 8.9, 4.4, 3.6, 3.7, 9, and 1.5, respectively (Fig. 7c). Talc is supersaturated in all water samples except three samples in NSSA (46, 48, and 52) showed negative value of SI. The supersaturation of calcium montmorillonite in 87 % of samples might be related to the dissolution of feldspar minerals, which produce ions that react with various minerals in water, forming montmorillonite. Aluminosilicate minerals weathering such as feldspar or mica can liberate aluminum ions, reacting with hydroxide ions in groundwater to generate gibbsite. The production of illite, kaolinite, k-mica, and k-feldspar in the two aquifers might be

attributed to the alteration of other minerals, such as feldspar weathering. Furthermore, hematite could arise from the oxidation of iron-bearing sediments in the aquifer. The supersaturation of chrysotile in water is related to the geological characteristics of the aquifers, such as the presence of magnesium silicate minerals. Chlorite could form through the breakdown and alteration of minerals in the aquifers, such as feldspars and micas. Fig. 8 shows the distribution map of the SI of the minerals in the water samples using the kriging method. The oversaturation of irrigation water in Siwa Oasis with minerals such as illite, kaolinite, and gibbsite can reduce soil permeability, decrease the infiltration rate, and increase the waterlogging. Additionally, the precipitation of the supersaturated minerals in the soil can alter its physical and chemical properties, leading to a decrease in soil fertility and crop productivity. However, rock minerals like chlorite, K-mica, K-feldspar, and hematite are more typically linked with hydrothermal systems and potentially indicate the presence of geothermal water at greater depths, but further research is needed. Siwa Oasis is located in a tectonically active environment with evidence of geothermal activity, such as hot springs and volcanic and metamorphic rocks.

The water temperature of the collected samples does not exceed 41.8 °C with a depth of 1040 m below sea level, which is not enough to confirm the presence of geothermal water, but the water temperature can be higher in greater depth where the NSSA lies above basement rocks at depth 3000 m below sea level. Fig. 8 showed the distribution maps of SI of some minerals saturated in the different groundwater resources in the Oasis. Exposure to the above supersaturated minerals in drinking water can lead to respiratory issues, skin irritation, digestive problems, and more severe health concerns like lung cancer, ovarian cancer, and other matters if ingested [67]. Physical and chemical treatment is required before the utilization of groundwater for drinking or irrigation purposes.

4.5. *Irrigation water quality indices*

To determine the impact of water quality on agricultural soils and the quality of crops, it is essential to study several vital indicators [68]. These indicators may be individual chemical indicators [69,70] or a group of indicators together [71–73]In the current study, some irrigation indices, such as SAR, Na%, MH, PS, and RSC, were calculated to evaluate irrigation water (Table 4).

Among all the elements present in the irrigation water, sodium ions have the most significant impact on agricultural soils, as high concentrations of sodium can decrease filtration rates by causing soil adsorption of sodium and removal of calcium and magnesium ions. Therefore, to assess water quality for agricultural irrigation, it is required to calculate the sodium adsorption ratio (SAR) and sodium percentage (Na%) indices based on sodium, calcium, and magnesium concentrations. This allows for the identification of areas where soil degradation is likely to occur. The water quality, as indicated by the SAR, was divided into four categories (Fig. 9). The majority of the samples (82.7 %) were classified as good to excellent with SAR values less than 18, including all NSSA samples, 20 samples from TCA, three samples of drain, and 3 samples of spring. On the other hand, the remaining samples (17.3 %) with SAR values greater than 18 were categorized as fair poor to unsuitable, which included 3 TCA samples, one spring sample, one drain sample, and all lake samples (Fig. 9). The Na% index values for surface and groundwater samples ranged from 24.5 to 71.3, with a mean value of 51.4. These samples were classified into three categories: 19.2 % were considered good, 55.8 % were permissible, and the rest (25 %) were considered doubtful. The samples with doubtful quality were found in 4 samples of TCA, four samples from NSSA, 4 samples of

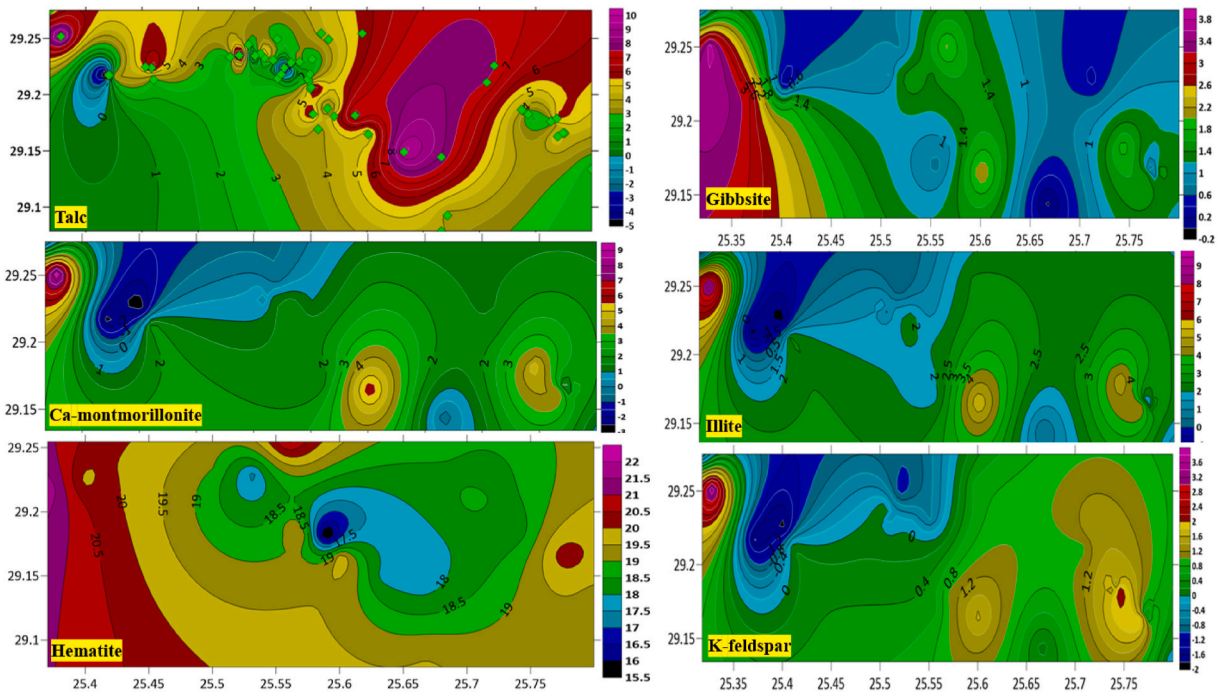

Fig. 8. Distribution map of the minerals extracted from the PHREEQC model based on SI value in the water samples.

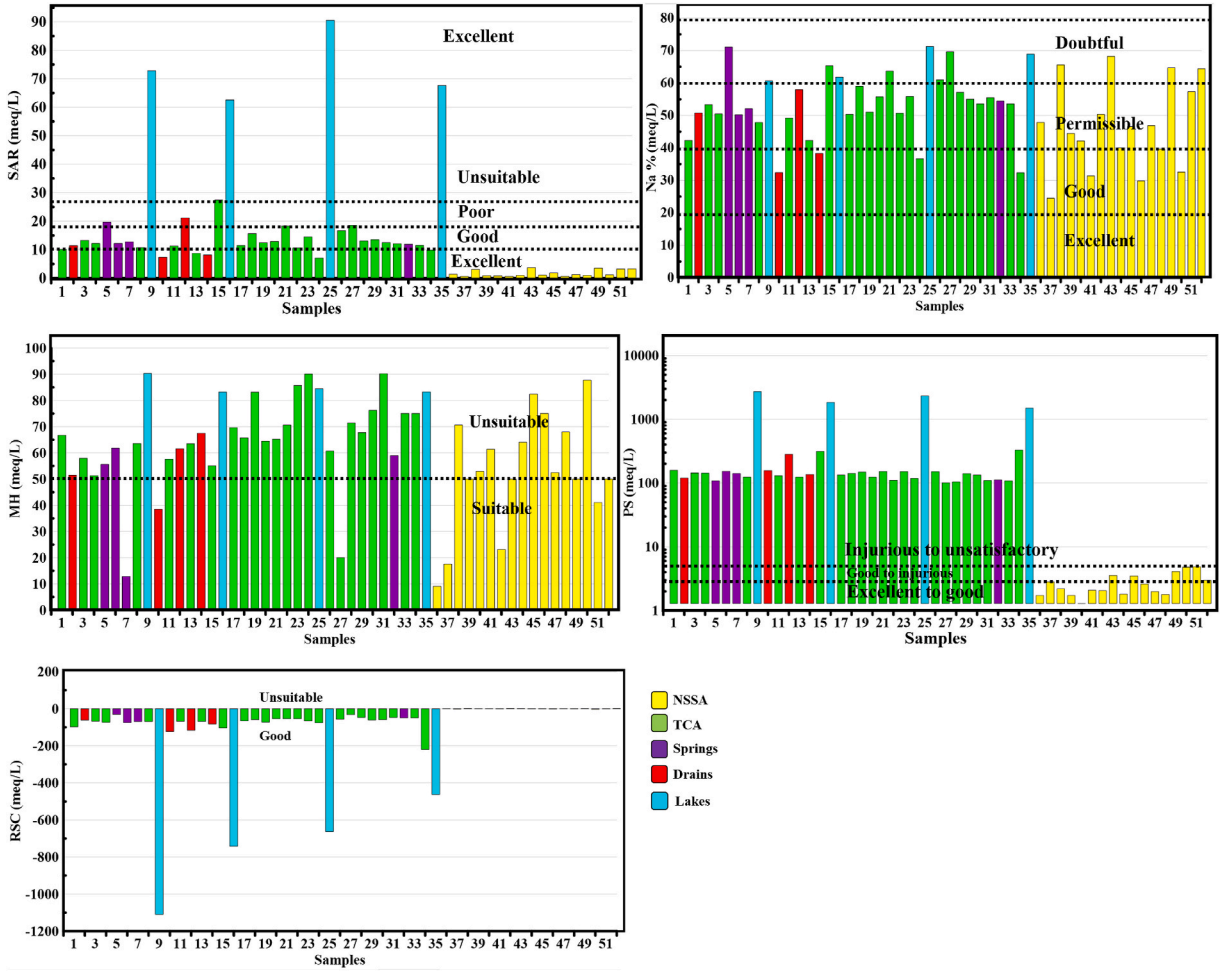

Fig. 9. Irrigation water quality indices of the water resources in Siwa Oasis.

salt lakes, and one spring sample (Fig. 9).

The TCA samples with high SAR and Na% values were located in the central Siwa Oasis near Aghormi and Siwa Lake, where the well depths ranged from 30 to 250 m BGL. The high SAR and Na% values in samples 15, 21, and 27, where cone of depression occurred in water levels, are expected to have an adverse effect on soil and plant production, which is supported by remote sensing and change detection showing a decrease in agricultural area and an increase in dry sabkha in these locations.

The MH value is an essential indicator of the appropriateness of water for agricultural purposes. High magnesium levels in irrigation water can lead to soil degradation, nutrient imbalances, and reduced crop yields, ultimately affecting the economic returns for farmers. In this study, the groundwater samples showed a mean MH value of 61.1, with 86.5 % of the samples having an MH value greater than 50 (Fig. 9). This indicates that the soil structure may degrade over time, leading to decreased permeability in the soil and contributing indirectly to waterlogging problems due to compacted soil.

The precipitation of alkali components such as magnesium and calcium can reduce irrigation water quality. This is a consequence of an increase in the content of bicarbonates and carbonates relative to magnesium and calcium in agricultural water. The residual sodium carbonate (RSC) index was estimated to determine water's appropriateness for irrigation. A significant increase in RSC concentration can cause the dissociation of organic matter and loss of soil structural characteristics, resulting in black stains on the soil's surface when dried. The RSC indicator's value was computed to estimate the likelihood of calcium and magnesium ions precipitating on soil surface particles and being removed from the soil solution. The majority of the water samples (98.1 %) in the study area were classified as good for irrigation based on the RSC indicator's results (Fig. 9). Another indicator used to assess the suitability of water for irrigation is the potential salinity index (PS). Using irrigation water with a high PS can lead to salt accumulation in the soil, resulting in reduced water availability, plant toxicity, and soil structure degradation, ultimately leading to reduced crop growth, yield, and quality, and lower economic returns for farmers. The Potential Salinity (PS) index is divided into three categories: Excellent to good ($PS < 3.0$), good to injurious ($PS = 3.0–5.0$), and Injurious to unsatisfactory ($PS > 5.0$). Results of the PS index indicate that 67.3 % of the water samples fall under the injurious to unsatisfactory category, including all surface water, springs, and TCA samples (Fig. 9). The rest of the samples belong to the good to excellent class, which represents all NSSA samples. The PS index value indicates that all water

samples from TCA can negatively affect soil properties and plant production.

4.6. The recommended plan for sustainable development

4.6.1. Subsurface drip irrigation (SDI)

Subsurface irrigation is watering plants where water is delivered directly to the root zone through buried pipes or porous tubing. In general, sandy soils with low clay content best suit subsurface irrigation. Loamy soils, which contain a mixture of sand, silt, and clay, can also work well for subsurface irrigation [74,75]. Fig. 10a illustrates the design of subsurface irrigation. The values of total sand in the studied area varied from 55.25 to 98.03 % (about 85 % on average). Silt content ranged between 0.02 and 36.23 % (about 8 % in average). Clay content varied from 1.34 to 22.40 % (about 7 % on average). Consequently, sandy soils are most prevalent in the studied area; however, small patches of clay soils are distributed in the area. The soil texture is loamy sand. Total carbonates content, represented as $CaCO_3$, ranged between 1.71 and 59.72 % (about 27 % on average) (Elnaggar et al., 2016). The physical characteristics of soil in Siwa oasis revealed that subsurface drip irrigation can be effectively applicable to the study area. The required water quantity for the crop evapotranspiration and the leaching is about 79 Mm^3/year for cultivating 10513 acres [50]. The total wells discharge was about 130 Mm^3/year [50]. The surface lakes receive 22 Mm3 of water annually from the surface drains as an excess water from agricultural areas.

The SDI can save up to 25 %–50 % of water as compared to surface irrigation by flooding [74,75]. The amount of water in Mm^3/year (X) that can be saved by applying subsurface drip irrigation was calculated as follows;

$X1 = 25*79/100 = 19.75\ Mm^3$/year

$X2 = 50*79/100 = 39.5\ Mm^3$/year

Where X1 represent saving 25 % of total irrigation water (79 Mm^3/year) and X2 refers to saving 50 %

The application of subsurface irrigation will have several advantages. First, it will decrease the amount of groundwater abstracted from TCA and NSSA, which will, hence, come upward of the water table and decrease the drawdown movement that causes deterioration of the water quality. Second, it will decrease the amount of water discharged into the salt lakes, which will, hence, stop increasing the surface area of the salt lakes. Third, it will prevent the water logging problem.

4.6.2. Removal of water logging by using perforated pipes under the soil

Perforated pipes (Fig. 10) can be used as a drainage system to remove excess water from waterlogged soil. The pipes are buried in the soil and are designed to allow water to enter the perforations and be transported away from the area through discharge in surface lining drains or canals. Using perforated pipes involves digging a trench in the affected area and placing the pipes at the bottom of the trench. The pipes are then covered with gravel or other porous materials, such as sand, to prevent soil from clogging the perforations.

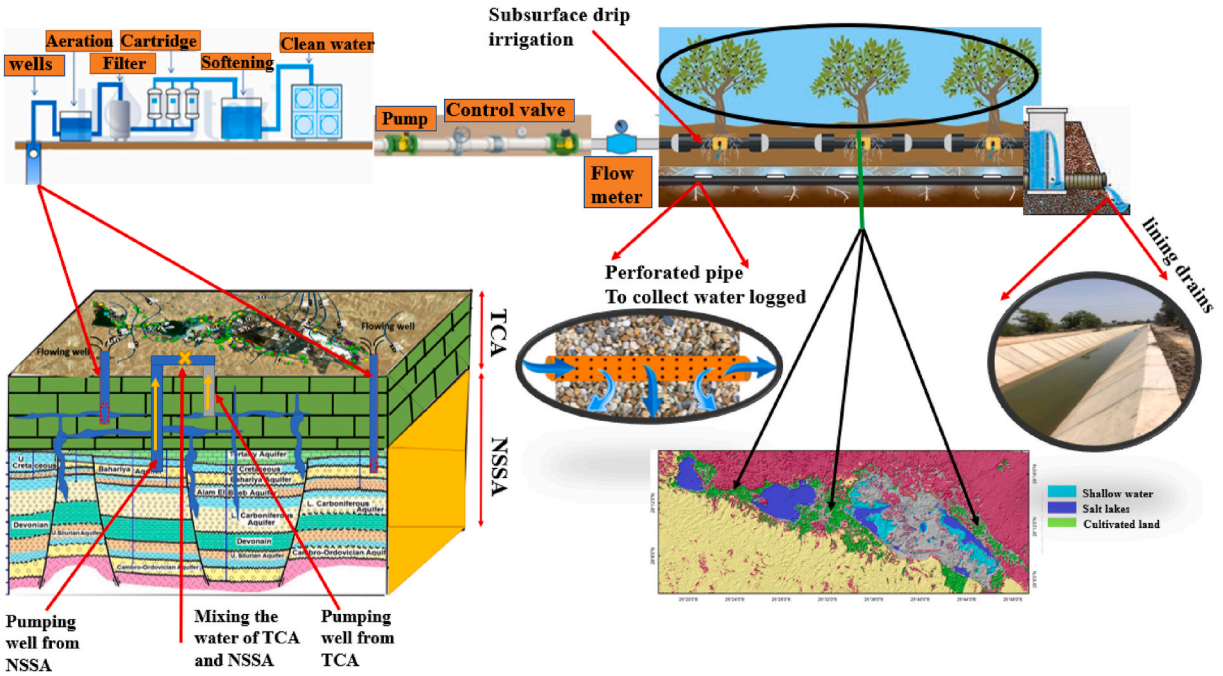

Fig. 10. Subsurface drip irrigation, perforated pipes, and mixing shallow water with deep aquifer for salinity reduction and sustainable development.

The trench is then filled with soil. As water accumulates in the soil, it enters the perforated pipes and is transported away from the area, which helps to remove the water logged in the soil.

4.6.3. Treatment of groundwater before irrigation

Groundwater must be treated before irrigation to decrease hardness and reduce the supersaturated minerals that can precipitate in the soil. The treatment requires aeration to precipitate iron and manganese-rich minerals, filtering to remove impurities and excess minerals, lime softening to precipitate calcium and magnesium ions, and reverse osmosis softening to reduce hardness.

4.6.4. Mixing the brackish water of TCA with fresh water of NSSA

Mixing the brackish water of TCA with fresh water of NSSA in pipes can decrease the salinity of water abstracted from TCA and make it suitable for irrigation through the dilution process. In the current study, the amount of freshwater required to mix with fresh water through pipe on the ground surface was calculated by the following equation;

$$TDS\ (mix) = (TDS1 \times V1 + TDS2 \times V2) / (V1 + V2)$$

where TDS1 is the TDS of the brackish water in TCA (average TDS = 8843 ppm), V1 is the volume of the brackish water required for cultivation (79 Mm^3/year), TDS2 is the TDS of the fresh water in the NSSA (average = 286 ppm), and V2 is the volume of the fresh water need to be added. The following equation calculated the volume (V2);

$$V2 = (TDS1 \times V1 - TDS2 \times V1) / (TDS2 - TDS\ (mix))$$

$V2 = (8843\ ppm \times 79{,}000{,}000\ m^3/year - 286\ ppm \times 79{,}000{,}000\ m^3/year)/(286\ ppm - TDS\ (mix))$

The desired TDS of the mixture to calculate V2 was proposed to be 1000 ppm in the mixture.

$V2 = (8843\ ppm \times 79{,}000{,}000\ m^3/year - 286\ ppm \times 79{,}000{,}000\ m^3/year)/(286\ ppm–1000\ ppm) = 6{,}200{,}723\ m^3/year.$

Therefore, approximately 6.2 million cubic meters of fresh water can be added to 79 million cubic meters of brackish water to achieve a TDS of 1000 ppm in the mixture. The volume of freshwater from the NSSA that can be saved by using subsurface drip irrigation can also be used for mixing.

5. Conclusion

The current research investigation assessed several problems endangering Siwa Oasis's sustainability, such as soil salinization, deterioration of water quality, water logging, depletion of nonchargeable water sources, and the provision of trustworthy solutions and water management strategies. The change detection in land cover revealed a substantial growth in the surface area of the saltwater lakes from 22.6 square kilometers in 1990 to 60.6 square kilometers in 2020. Because of the salinization of the soil and waterlogged waters, the cultivated land of the Siwa Oasis has transformed into dry sabkha, particularly in the central Siwa. Evaluation of the water salinity from 1998 to 2022 revealed a dramatic decline in the TCA's groundwater quality due to increased water withdrawal for irrigation. The pressure-depth profile demonstrated that the groundwater in NSSA is above hydrostatic pressure in the investigated area's eastern and western parts. In contrast, the pressure in the region's center has decreased to below hydrostatic pressure, indicating upward groundwater movement in the eastern and western parts. In the center section of the Oasis, the vertical movement altered downward, which could explain the increase in water salinity in the TCA due to decreased TCA recharging from the NSSA as well as seepage of water from hypersaline lakes to the shallow aquifer. The Chadha and piper plots revealed that the water type altered upward from Ca–Mg–HCO_3 in the deep aquifer (NSSA) to Na–Cl in the shallow aquifer (TCA) and surface water. The irrigation water has the ability to precipitate the supersaturated minerals in the soil which decreases the permeability of the soil and prevents excess water from infiltration creating water logging problems. The irrigation indices suggested that NSSA is appropriate for agriculture. However, TCA is not appropriate for irrigation due to MH and PS. The water quality according to SAR, and Na% range from good to doubtful while it fell in good category regarding RSC index. Environmental sustainability and management of water resources necessitate water treatment, underground drip irrigation, a perforated pipeline system, and a mixture of TCA and NSSA water.

Funding

The current research work has been funded by the sustainable development and technologies national program of the Hungarian Academy of Sciences (FFT NP FTA). Also, the authors extend their appreciation to King Saud University for funding this work through Researchers Supporting Project number (RSP2024R133), King Saudia University, Riyadh, Saudia Arabia.

Data availability

The data used in this research are available by the corresponding author upon reasonable request.

CRediT authorship contribution statement

Mohamed Hamdy Eid: Writing – review & editing, Writing – original draft, Visualization, Validation, Software, Methodology, Investigation, Formal analysis, Data curation, Conceptualization. **Ali Shebl:** Writing – original draft, Visualization, Software, Data

curation. **Mustafa Eissa:** Writing – review & editing, Resources, Investigation, Formal analysis. **Essam A. Mohamed:** Writing – review & editing, Validation, Investigation, Formal analysis. **Amr S. Fahil:** Writing – review & editing, Validation, Conceptualization. **Hatem Saad Ramadan:** Writing – review & editing, Resources, Investigation, Formal analysis. **Mostafa R. Abukhadra:** Writing – review & editing, Software, Data curation, Conceptualization. **Ahmed M. El-Sherbeeny:** Writing – review & editing, Software, Funding acquisition. **Attila Kovacs:** Writing – review & editing, Supervision, Formal analysis, Conceptualization. **Péter Szűcs:** Writing – review & editing, Supervision, Project administration, Funding acquisition, Formal analysis, Conceptualization.

Declaration of competing interest

The authors declare that they have no known competing financial interests or personal relationships that could have appeared to influence the work reported in this paper.

Acknowledgements

We would like to thank the desert research center for helping to collect the water samples. The current research work has been funded by **the sustainable development and technologies national program of the Hungarian Academy of Sciences (FFT NP FTA).** Also, the authors extend their appreciation to King Saud University for funding this work through Researchers Supporting Project number (RSP2024R133), King Saud University, Riyadh, Saudi Arabia.

Appendix A. Supplementary data

Supplementary data to this article can be found online at https://doi.org/10.1016/j.heliyon.2024.e32992.

References

[1] E. Ghoneim, C. Healey, M. Hemida, A. Shebl, A. Fahil, Integration of Geophysical and Geospatial Techniques to Evaluate Geothermal Energy at Siwa Oasis vol 15, Remote Sensing, Western Desert, Egypt, 2023, p. 5094, https://doi.org/10.3390/rs15215094.
[2] S. Elsayed, M. Gupta, G. Chaudhary, S. Taneja, H. Gaur, M. Gad, M. Hamdy Eid, A. Kovács, S. Péter, A. Gaagai, et al., Interpretation the influence of Hydrometeorological Variables on soil temperature prediction using the potential of deep learning model, Kbes 4 (2023) 55–77, https://doi.org/10.51526/kbes.2023.4.1.55-77.
[3] M.R. Abukhadra, M.H. Eid, M.A. El-Meligy, M. Sharaf, A.T. Soliman, Insight into Chitosan/Mesoporous Silica Nanocomposites as eco-friendly adsorbent for enhanced retention of U (VI) and Sr (II) from aqueous solutions and real water, Int. J. Biol. Macromol. 173 (2021) 435–444, https://doi.org/10.1016/j.ijbiomac.2021.01.136.
[4] S. Bellucci, M.H. Eid, I. Fekete, S. Péter, A. Kovács, S.I. Othman, J.S. Ajarem, A.A. Allam, M.R. Abukhadra, Synthesis of K+ and Na+ synthetic sodalite phases by low-temperature alkali fusion of kaolinite for effective remediation of phosphate ions: the impact of the alkali ions and realistic studies, INORGA 11 (2022) 14, https://doi.org/10.3390/inorganics11010014.
[5] P. Szucs, M. Dobróka, E. Turai, L. Szarka, C. Ilyés, M.H. Eid, N.P. Szabó, Combined inversion and statistical workflow for advanced temporal analysis of the nile river's long term water level records, J. Hydrol. 630 (2024) 130693, https://doi.org/10.1016/j.jhydrol.2024.130693.
[6] N.P. Szabó, C. Ilyés, E. Turai, M. Dobróka, R. Kilik, R. Miklós, M.H. Eid, P. Szücs, Fourier transformation and unsupervised learning for extracting hydrogeological information from time series data, in: Proceedings of the 2023 14th IEEE International Conference on Cognitive Infocommunications (CogInfoCom), IEEE, Budapest, Hungary, September 22 2023, 000019–000024.
[7] M.H. Eid, M. Eissa, E.A. Mohamed, H.S. Ramadan, G. Czuppon, A. Kovács, P. Szucs, Application of stable isotopes, mixing models, and K-means cluster analysis to detect recharge and salinity origins in Siwa oasis, Egypt, Groundwater for Sustainable Development 25 (2024) 101124, https://doi.org/10.1016/j.gsd.2024.101124.
[8] A.A.E.-S.M. Ata, M.H. Aly, H. Hussein, M.H. Eid, M.R. Abukhadra, A.M. El-Sherbeeny, S. Bellucci, M. Gad, Hydrogeochemical characteristics and air quality risks associated with gold mining operations in Egypt using geochemical modeling and risk indices, Heliyon 10 (2024) e31086, https://doi.org/10.1016/j.heliyon.2024.e31086.
[9] M.H. Eid, M. Eissa, E.A. Mohamed, H.S. Ramadan, M. Tamás, A. Kovács, P. Szucs, New approach into human health risk assessment associated with heavy metals in surface water and groundwater using Monte Carlo method, Sci. Rep. 14 (2024) 1008, https://doi.org/10.1038/s41598-023-50000-y.
[10] M.H. Al-Mashreki, M.H. Eid, O. Saeed, A. Székács, P. Szucs, M. Gad, M.R. Abukhadra, A.A. AlHammadi, M.S. Alrakhami, M.A. Alshabibi, et al., Integration of geochemical modeling, multivariate analysis, and irrigation indices for assessing groundwater quality in the Al-jawf basin, Yemen, Water 15 (2023) 1496, https://doi.org/10.3390/w15081496.
[11] F.P. Salcedo, P.P. Cutillas, J.J.A. Cabañero, A.G. Vivaldi, Use of remote sensing to evaluate the effects of environmental factors on soil salinity in a semi-arid area, Sci. Total Environ. 815 (2022) 152524, https://doi.org/10.1016/j.scitotenv.2021.152524.
[12] X. Yin, Q. Feng, Y. Li, R.C. Deo, W. Liu, M. Zhu, X. Zheng, R. Liu, An interplay of soil salinization and groundwater degradation threatening coexistence of oasis-desert ecosystems, Sci. Total Environ. 806 (2022) 150599, https://doi.org/10.1016/j.scitotenv.2021.150599.
[13] M.A. Salam, A. Adlii, M.H. Eid, M.R. Abukhadra, Effective decontamination of Ca2+ and Mg2+ hardness from groundwater using innovative muscovite based sodalite in batch and fixed-bed column studies; dynamic and equilibrium studies, J. Contam. Hydrol. 241 (2021) 103817, https://doi.org/10.1016/j.jconhyd.2021.103817.
[14] M.R. Abukhadra, M.H. Eid, A.M. El-Sherbeeny, A.E.E. Abd Elgawad, J.-J. Shim, Effective desalination of brackish groundwater using zeolitized diatomite/kaolinite geopolymer as low-cost inorganic membrane; Siwa oasis in Egypt as a realistic case study, J. Contam. Hydrol. 244 (2022) 103923, https://doi.org/10.1016/j.jconhyd.2021.103923.
[15] M.N. Bin Jumah, M.H. Eid, A.A. Al-Huqail, M.A. Mohammad, N.S. Bin-Murdhi, G.M. Abu-Taweel, N. Altoom, A.A. Allam, M.R. AbuKhadra, Enhanced remediation of as (V) and Hg (II) ions from aqueous environments using β-cyclodextrin/MCM-48 composite: batch and column studies, J. Water Proc. Eng. 42 (2021) 102118, https://doi.org/10.1016/j.jwpe.2021.102118.
[16] M. Hamdy Eid, P. Szucs, A. Kovács, Problems threatening sustainability in Siwa oasis and recommendations for understanding the sources of water quality deterioration, Geosciences and Engineering 10 (2022) 138–153, https://doi.org/10.33030/geosciences.2022.15.138.
[17] A.A. Madani, Soil salinity detection and monitoring using Landsat data: a case study from Siwa oasis, Egypt, GIScience Remote Sens. 42 (2005) 171–181, https://doi.org/10.2747/1548-1603.42.2.171.

[18] A.A. Aly, F.M. Kishk, H.M. Gaber, A.M. Al-Omran, Long-term detection and hydrochemistry of groundwater resources in Egypt: case study of Siwa oasis, Journal of the Saudi Society of Agricultural Sciences 15 (2016) 67–74, https://doi.org/10.1016/j.jssas.2014.04.003.

[19] R. Goossens, E. Van Ranst, The use of remote sensing to map gypsiferous soils in the ismailia province (Egypt), Geoderma 87 (1998) 47–56, https://doi.org/10.1016/S0016-7061(98)00069-X.

[20] D. Deming, Introduction to Hydrogeology, McGraw-Hill Science, Engineering & Mathematics, 2002, 0-07-232622-0.

[21] S.E. Ingebritsen, W.E. Sanford, C.E. Neuzil, Groundwater in Geologic Processes, Cambridge university press, 2006, 1-00-924749-2.

[22] J. Mádl-Szőnyi, S. Simon, Involvement of preliminary regional fluid pressure evaluation into the reconnaissance geothermal exploration—example of an overpressured and gravity-driven basin, Geothermics 60 (2016) 156–174, https://doi.org/10.1016/j.geothermics.2015.11.001.

[23] L. Lenkey, P. Dövényi, F. Horváth, S. Cloetingh, Geothermics of the pannonian basin and its bearing on the neotectonics, EGU Stephan Mueller Special Publication Series 3 (2002) 29–40.

[24] J. Tóth, The Double Sources of Thermal Waters Int He Hungarian Great Plain and Its Practical Consequences: A Hypothesis Based on Observations. Geothermics and Environmental Industry in the 21st Century, Conference. Kistelek (2006).

[25] N. Subba Rao, A. Dinakar, L. Sun, Estimation of groundwater pollution levels and specific ionic sources in the groundwater, using a comprehensive approach of geochemical ratios, pollution index of groundwater, unmix model and land use/land cover – a case study, J. Contam. Hydrol. 248 (2022) 103990, https://doi.org/10.1016/j.jconhyd.2022.103990.

[26] N. Subba Rao, R. Das, H.K. Sahoo, S. Gugulothu, Hydrochemical characterization and water quality perspectives for groundwater management for urban development, Groundwater for Sustainable Development 24 (2024) 101071, https://doi.org/10.1016/j.gsd.2023.101071.

[27] R. Das, N. Subba Rao, H.K. Sahoo, G. Sakram, Nitrate contamination in groundwater and its health implications in a semi-urban region of titrol block, jagatsinghpur district, odisha, India, Phys. Chem. Earth, Parts A/B/C 132 (2023) 103424, https://doi.org/10.1016/j.pce.2023.103424.

[28] A. Gaagai, H. Aouissi, S. Bencedira, G. Hinge, A. Athamena, S. Heddam, M. Gad, O. Elsherbiny, S. Elsayed, M. Eid, et al., Application of water quality indices, machine learning approaches, and GIS to identify groundwater quality for irrigation purposes: a case study of sahara aquifer, doucen plain, Algeria, Water 15 (2023) 289, https://doi.org/10.3390/w15020289.

[29] S. Salem, A. Gaagai, I. Ben Slimene, A. Moussa, K. Zouari, K. Yadav, M. Eid, M. Abukhadra, A. El-Sherbeeny, M. Gad, et al., Applying multivariate analysis and machine learning approaches to evaluating groundwater quality on the Kairouan plain, Tunisia, Water 15 (2023) 3495, https://doi.org/10.3390/w15193495.

[30] O. Saeed, A. Székács, G. Jordán, M. Mörtl, M.R. Abukhadra, M.H. Eid, Correction: investigating the impacts of heavy metal(loid)s on ecology and human health in the lower basin of Hungary's danube river: a Python and Monte Carlo simulation-based study, Environ. Geochem. Health 45 (2023) 9785, https://doi.org/10.1007/s10653-023-01777-4, 9785.

[31] H. Ibrahim, Z.M. Yaseen, M. Scholz, M. Ali, M. Gad, S. Elsayed, M. Khadr, H. Hussein, H.H. Ibrahim, M.H. Eid, et al., Evaluation and prediction of groundwater quality for irrigation using an integrated water quality indices, machine learning models and GIS approaches: a representative case study, Water 15 (2023) 694, https://doi.org/10.3390/w15040694.

[32] M.H. Eid, M. Elbagory, A.A. Tamma, M. Gad, S. Elsayed, H. Hussein, F.S. Moghanm, A.E.-D. Omara, A. Kovács, S. Péter, Evaluation of groundwater quality for irrigation in deep aquifers using multiple graphical and indexing approaches supported with machine learning models and GIS techniques, souf valley, Algeria, Water 15 (2023) 182, https://doi.org/10.3390/w15010182.

[33] M. Gad, A. Gaagai, M.H. Eid, P. Szűcs, H. Hussein, O. Elsherbiny, S. Elsayed, M.M. Khalifa, F.S. Moghanm, M.E. Moustapha, et al., Groundwater quality and health risk assessment using indexing approaches, multivariate statistical analysis, artificial neural networks, and GIS techniques in El kharga oasis, Egypt, Water 15 (2023) 1216, https://doi.org/10.3390/w15061216.

[34] Y.G. Flores, M.H. Eid, P. Szűcs, T. Szőcs, T. Fancsik, J. Szanyi, B. Kovács, G. Markos, P. Újlaki, P. Tóth, et al., Integration of geological, geochemical modelling and hydrodynamic condition for understanding the geometry and flow pattern of the aquifer system, southern nyírség–Hajdúság, Hungary, Water 15 (2023) 2888, https://doi.org/10.3390/w15162888.

[35] C.E. Moya, M. Raiber, M. Taulis, M.E. Cox, Hydrochemical evolution and groundwater flow processes in the galilee and eromanga basins, Great Artesian basin, Australia: a multivariate statistical approach, Sci. Total Environ. 508 (2015) 411–426, https://doi.org/10.1016/j.scitotenv.2014.11.099.

[36] M.H. Al-Mashreki, M.H. Eid, O. Saeed, A. Székács, P. Szűcs, M. Gad, M.R. Abukhadra, A.A. AlHammadi, M.S. Alrakhami, M.A. Alshabibi, et al., Integration of geochemical modeling, multivariate analysis, and irrigation indices for assessing groundwater quality in the Al-jawf basin, Yemen, Water 15 (2023) 1496, https://doi.org/10.3390/w15081496.

[37] P.A. Domenico, F.W. Schwartz, Physical and Chemical Hydrogeology, John wiley & sons, 1997, 0-471-59762-7.

[38] K.W.F. Howard, P. Beck, Hydrochemical interpretation of groundwater flow systems in quaternary sediments of southern ontario, Can. J. Earth Sci. 23 (1986) 938–947, https://doi.org/10.1139/e86-095.

[39] A. Gautam, S.C. Rai, Groundwater zoning and sustainable management strategies for groundwater resources in the bist-doab region of Punjab, India, Environ. Dev. Sustain. (2023), https://doi.org/10.1007/s10668-023-03053-y.

[40] H. Sinha, S.C. Rai, S. Kumar, Post-monsoon groundwater hydrogeochemical characterization and quality assessment using geospatial and multivariate analysis in chhotanagpur plateau, India, Environ. Dev. Sustain. (2023), https://doi.org/10.1007/s10668-023-03459-8.

[41] M.H. Eid, M. Elbagory, A.A. Tamma, M. Gad, S. Elsayed, H. Hussein, F.S. Moghanm, A.E.-D. Omara, A. Kovács, S. Péter, Evaluation of groundwater quality for irrigation in deep aquifers using multiple graphical and indexing approaches supported with machine learning models and GIS techniques, souf valley, Algeria, Water 15 (2023) 182, https://doi.org/10.3390/w15010182.

[42] A. Gaagai, H.A. Aouissi, S. Bencedira, G. Hinge, A. Athamena, S. Haddam, M. Gad, O. Elsherbiny, S. Elsayed, M.H. Eid, et al., Application of water quality indices, machine learning approaches, and GIS to identify groundwater quality for irrigation purposes: a case study of sahara aquifer, doucen plain, Algeria, Water 15 (2023) 289, https://doi.org/10.3390/w15020289.

[43] S. Gugulothu, N. Subbarao, R. Das, R. Dhakate, Geochemical evaluation of groundwater and suitability of groundwater quality for irrigation purpose in an agricultural region of south India, Appl. Water Sci. 12 (2022) 142, https://doi.org/10.1007/s13201-022-01583-w.

[44] P. Aravinthasamy, D. Karunanidhi, N. Subba Rao, T. Subramani, K. Srinivasamoorthy, Irrigation risk assessment of groundwater in a non-perennial river basin of south India: implication from irrigation water quality index (IWQI) and geographical information system (GIS) approaches, Arabian J. Geosci. 13 (2020) 1125, https://doi.org/10.1007/s12517-020-06103-1.

[45] S.A. El-Sayed, K.A. Allam, M.H. Salama, H. El Begawy, Investigation of chemical and radiochemical fingerprints of water resources in Siwa oasis, western desert, Egypt, Arab Journal of Nuclear Science and Applications 50 (2017) 158–178.

[46] A. Abdallah, Assessment of salt weathering in Siwa oasis (the western desert of Egypt), Bull. De la Soc. De Geog. De Egypt 80 (2007) 66–83.

[47] S.M. Abdel-Mogheeth, Groundwater hazards in Siwa oasis, Ground water protection (1996) 113–118.

[48] A.H. Afifi, Assessment of the Hydrogeological Conditions of Groundwater in Siwa Oasis, North Western Desert vol 98p, Minufiya University, Egypt, 2005. Ph. D. Thesis.

[49] K.A. Dahab, Impact of the present groundwater exploitation system on the nubia sandstone aquifer in Siwa oasis, western desert, Egypt. 6th intern, in: Proceedings of the Conf. On Geochemistry, Alex, Univ., Egypt, 2004, pp. 319–337.

[50] M.F.M. El Hossary, Investigating the development challenges to Siwa oasis, northwestern desert, Egypt, N. Sci. J 6 (2013) 55–61.

[51] T.A. Aggour, A.M. Faid, Hydrogeology of Siwa oasis and landuse map, Egypt, J Remote Sens Space Sci 9 (2007) 135–156.

[52] A.M. Abdulaziz, A.M. Faid, Evaluation of the groundwater resources potential of Siwa oasis using three-dimensional multilayer groundwater flow model, mersa matruh governorate, Egypt, Arabian J. Geosci. 8 (2015) 659–675, https://doi.org/10.1007/s12517-013-1199-4.

[53] L.A. Richards, Diagnosis and Improvement of Saline and Alkali Soils, vol 78, LWW, 1954, 0038-075X.

[54] H.M. Raghunath, Groundwater, Wiley Eastern Ltd, New Delhi, India, 1987.

[55] L.D. Doneen, *Notes On Water Quality In Agriculture*; Department of Water Science and Engineering, University of California, Davis, 1964.

[56] A. Shebl, M. Abdellatif, M. Hissen, M. Ibrahim Abdelaziz, Á. Csámer, Lithological mapping enhancement by integrating sentinel 2 and gamma-ray data utilizing support vector machine: a case study from Egypt, Int. J. Appl. Earth Obs. Geoinf. 105 (2021) 102619, https://doi.org/10.1016/j.jag.2021.102619.

[57] C. Kumar, S. Chatterjee, T. Oommen, A. Guha, Automated lithological mapping by integrating spectral enhancement techniques and machine learning algorithms using AVIRIS-NG hyperspectral data in gold-bearing granite-greenstone rocks in hutti, India, Int. J. Appl. Earth Obs. Geoinf. 86 (2020) 102006, https://doi.org/10.1016/j.jag.2019.102006.
[58] A. Shebl, M.I. Abdelaziz, H. Ghazala, S.A.S. Araffa, M. Abdellatif, Á. Csámer, Multi-criteria ground water potentiality mapping utilizing remote sensing and geophysical data: a case study within sinai peninsula, Egypt, The Egyptian Journal of Remote Sensing and Space Science 25 (2022) 765–778, https://doi.org/10.1016/j.ejrs.2022.07.002.
[59] G.P. Petropoulos, C. Kalaitzidis, K. Prasad Vadrevu, Support vector machines and object-based classification for obtaining land-use/cover cartography from hyperion hyperspectral imagery, Comput. Geosci. 41 (2012) 99–107, https://doi.org/10.1016/j.cageo.2011.08.019.
[60] V. Chaplot, F. Darboux, H. Bourennane, S. Leguédois, N. Silvera, K. Phachomphon, Accuracy of interpolation techniques for the derivation of digital elevation models in relation to landform types and data density, Geomorphology 77 (2006) 126–141, https://doi.org/10.1016/j.geomorph.2005.12.010.
[61] X. Ding, J. Liu, F. Yang, J. Cao, Random radial basis function kernel-based support vector machine, J. Franklin Inst. 358 (2021) 10121–10140, https://doi.org/10.1016/j.jfranklin.2021.10.005.
[62] M.K. Hubbert, The theory of ground-water motion, J. Geol. 48 (1940) 785–944, https://doi.org/10.1086/624930.
[63] R. Ayers, D. Westcott, Water quality for agriculture. FAO Irrigation and Drainage Paper 29 Rev. 1, Food and Agricultural Organisation of the United Nations, 1994.
[64] W.H. Organization, WHO *Guidelines for drinking-water quality*, World Health Organization 1 (2004), 92-4-154638-7.
[65] A.M.A. Piper, Graphic procedure in the geochemical interpretation of water-analyses, Trans. AGU 25 (1944) 914, https://doi.org/10.1029/TR025i006p00914.
[66] D.K. Chadha, A proposed new diagram for geochemical classification of natural waters and interpretation of chemical data, Hydrogeol. J. 7 (1999) 431–439, https://doi.org/10.1007/s100400050216.
[67] P. Sengupta, Potential health impacts of hard water, Int. J. Prev. Med. 4 (2013) 866.
[68] N.S. Rao, A. Dinakar, M. Sravanthi, B.K. Kumari, Geochemical characteristics and quality of groundwater evaluation for drinking, irrigation, and industrial purposes from a part of hard rock aquifer of south India, Environ. Sci. Pollut. Res. 28 (2021) 31941–31961, https://doi.org/10.1007/s11356-021-12404-z.
[69] N.S. Kawo, S. Karuppannan, Groundwater quality assessment using water quality index and GIS technique in modjo river basin, Central Ethiopia, J. Afr. Earth Sci. 147 (2018) 300–311, https://doi.org/10.1016/j.jafrearsci.2018.06.034.
[70] P. Li, J. Wu, H. Qian, Assessment of groundwater quality for irrigation purposes and identification of hydrogeochemical evolution mechanisms in pengyang county, China, Environ. Earth Sci. 69 (2013) 2211–2225, https://doi.org/10.1007/s12665-012-2049-5.
[71] A.C.M. Meireles, E.M. de Andrade, L.C.G. Chaves, H. Frischkorn, L.A. Crisostomo, A new proposal of the classification of irrigation water, Rev. Cienc. Agron. 41 (2010) 349–357, https://doi.org/10.1590/S1806-66902010000300005.
[72] F. Misaghi, F. Delgosha, M. Razzaghmanesh, B. Myers, Introducing a water quality index for assessing water for irrigation purposes: a case study of the ghezel ozan river, Sci. Total Environ. 589 (2017) 107–116, https://doi.org/10.1016/j.scitotenv.2017.02.226.
[73] R. RamyaPriya, L. Elango, Evaluation of geogenic and anthropogenic impacts on spatio-temporal variation in quality of surface water and groundwater along cauvery river, India, Environ. Earth Sci. 77 (2018) 2, https://doi.org/10.1007/s12665-017-7176-6.
[74] M.A. Abou Seeda, S.A. Hammad, A.A. Yassen, E.A. Abou El-Nour, Evaluation and optimization of subsurface irrigation (sdi) system: a review, Middle East Journal of Applied Sciences 10 (2020) 508–538.
[75] Y. Liu, C. Hu, B. Li, D. Ding, Z. Zhao, T. Fan, Z. Li, Subsurface drip irrigation reduces cadmium accumulation of pepper (capsicum annuum L.) plants in upland soil, Sci. Total Environ. 755 (2021) 142650, https://doi.org/10.1016/j.scitotenv.2020.142650.